Available online at www.sciencedirect.com

ScienceDirect

Geochimica et Cosmochimica Acta 259 (2019) 211–232

Geochimica et Cosmochimica Acta

www.elsevier.com/locate/gca

Inorganic and organic iron and copper species of the subterranean estuary: Origins and fate

Hannelore Waska [a,*], Hans-Jürgen Brumsack [b], Gudrun Massmann [c], Andrea Koschinsky [d], Bernhard Schnetger [b], Heike Simon [a], Thorsten Dittmar [a,e]

[a] *Research Group for Marine Geochemistry (ICBM-MPI Bridging Group), Institute for Chemistry and Biology of the Marine Environment (ICBM), University of Oldenburg, Oldenburg, Germany*

[b] *Microbiogeochemistry Group, Institute for Chemistry and Biology of the Marine Environment (ICBM), University of Oldenburg, Oldenburg, Germany*

[c] *Hydrogeology and Landscape Hydrology Group, Institute for Biology and Environmental Sciences (IBU), University of Oldenburg, Oldenburg, Germany*

[d] *Jacobs University Bremen, Earth and Space Sciences, Bremen, Germany*

[e] *Helmholtz Institute for Functional Marine Biodiversity (HIFMB), University of Oldenburg, Oldenburg, Germany*

Received 10 April 2018; accepted in revised form 3 June 2019; available online 15 June 2019

Abstract

Subterranean estuaries (STEs) are land-ocean interfaces where meteoric fresh groundwater mixes with intruding seawater in a coastal aquifer, before discharging into the adjacent water column. In contrast to surface estuaries, STEs have the potential to amplify concentrations of constituents such as copper (Cu) and iron (Fe) due to long residence times and reductive dissolution of mineral phases along the groundwater flowpaths. However, oxidative precipitation of Fe and Mn at the sediment-water interface may scavenge many constituents again before they reach the coastal water column. Hence, the geochemical impact of the suboxic to anoxic submarine groundwater discharge (SGD) on the oxygenated coastal ocean relies on the capability of constituents such as Cu and Fe to stay in solution across redox boundaries. Here, we propose that dissolved organic matter (DOM) in the STE plays a pivotal role in the speciation of Cu and Fe through (i) fueling reductive dissolution and (ii) providing ligands to form stable metal-DOM complexes, increasing their transfer from the STE into the coastal ocean. We investigated the concentrations and speciation of Cu and Fe, and DOM chemical characteristics, in two beach STEs of a barrier island. By combining well-established techniques with novel quantification and speciation approaches from both the inorganic and organic geochemical realm (size-fractionation filtration, ferrozine detection, voltammetry, sequential DOM extraction, and ultra-high resolution mass spectrometry) we characterized metal-DOM associations down to the molecular level. Overall, pore water from both STEs was enriched with Cu and Fe compared to seawater, which indicated transfer potential for both trace metals across the sediment-water interface. However, Fe gradients from pore water to surface were steeper than those for Cu, indicating a larger net transfer of the latter compared to the former. Our voltammetry data showed that Cu was exclusively organically bound in both STEs and the water column, mostly in soluble form (<20 nm). The majority of >60 newly identified Cu-containing complexes had primarily aliphatic character and N and S in their molecular formulae resembling labile marine DOM, while two Cu-DOM complexes had polyphenol ("humic-like") molecular formulae indicative of terrestrial vascular plant-derived material. In contrast to Cu, the Fe pool consisted of either reduced, soluble (<20 nm), likely free Fe(II) in the anoxic STE, or of larger colloids (<200 nm and >20 nm) in the fresh groundwater and seawater end-members, likely as Fe(III)(hydr)oxides stabilized by DOM. Furthermore, while Fe and humic-like DOM seemed to share common sources, all directly identified mobile Fe-DOM complexes appeared to have marine origins. Therefore, organic forms

* Corresponding author.
E-mail address: hannelore.waska@uni-oldenburg.de (H. Waska).

https://doi.org/10.1016/j.gca.2019.06.004

of Fe in the STE may primarily consist of immobile humic-Fe coagulates, partially mobile Fe-nanocolloids, and mobile, N-containing, marine aliphatic Fe-complexes. Our study indicates that aliphatic, N-containing ligands may play an important role in the organic complexation and stabilization of Fe and particularly Cu in the STE, and enable them to cross redox boundaries at the sediment-water interface.

Keywords: Copper; Iron; DOM; Subterranean estuary; Ligands; Complex; Groundwater; Sea water

1. INTRODUCTION

The subterranean estuary (STE) is a biogeochemically reactive underground transition zone between land and sea, where fresh, meteoric groundwater mixes with tidally- and wave- recirculated seawater. STEs are of particular importance in unconfined coastal aquifers such as sandy beach sediments, where long groundwater residence times enable thorough processing of introduced terrestrially- and marine-derived organic matter by active microbial communities (Moore, 1999, Seidel et al., 2015). Through the microbial remineralization driven by supply of electron donors and acceptors *via* advective ground- and porewater flow, the STE can change the concentration and speciation of terrestrially- and marine-derived chemical constituents before submarine groundwater is discharged into the coastal ocean (SGD, Moore, 1996). During passage through the STE, pore water may become enriched compared to the overlying water column, with chemical constituents such as nitrate and silicate (Waska and Kim, 2011), dissolved organic carbon (DOC; Kim et al., 2012), barium and radium (Charette and Sholkovitz, 2006), rare earth elements (REE; Johannesson et al., 2011) and other trace elements, such as copper and iron (Cu and Fe, Montluçon and Sañudo-Wilhelmy, 2001, Windom et al., 2006). SGD occurs ubiquitously worldwide (Zhang and Mandal, 2012), and on a global scale, its volumetric and constituent fluxes are estimated to be in the same order of magnitude as that of rivers (Burnett et al., 2003, Kwon et al., 2014, Cho and Kim, 2016, Cho et al., 2018).

The extent of SGD's geochemical impact on the nearby coastal water column depends not only on the accumulation of chemical constituents within the STE, but also on the stability of these constituents during transit across the sediment-water interface. For example, SGD is often enriched in reduced Fe(II) (Snyder et al., 2004, Windom et al., 2006, Roy et al., 2013), but the propagation of an SGD-induced Fe signal in the coastal ocean may be geographically limited due to rapid oxidative precipitation (Windom et al., 2006). It has been hypothesized that reduced Fe and Cu released from sediments and hydrothermal vents are stabilized in the open water column by ubiquitously occurring organic metal-binding ligands (Windom et al., 2006; Sander and Koschinsky, 2011). Correspondingly, dissolved organic matter (DOM) in the STE could provide a mobile carrier for trace elements such as Fe and REEs across redox boundaries, in the form of colloids or dissolved complexes (Windom et al., 2006, Beck et al., 2010, Johannesson et al., 2011, Kim and Kim, 2015).

However, very little is known about the nature of metal-DOM compounds in the STE to date. Nickel (Ni), Cu, and manganese (Mn) are associated with DOM in substantial amounts: Beck et al. (2010) reported the occurrence of organic Ni and Cu in the STE, which were isolated by targeting their complexing organic ligands *via* solid-phase extraction (SPE). Kim and Kim (2015) linked abundances of dissolved Mn and polonium-210 (^{210}Po) to the occurrence of colloidal DOM, which was defined as the fraction isolated between a 0.45 μm and a 10 kDa filter. Nevertheless, it is not well known which chemical fractions of DOM are involved in metal binding in the STE, and where they may originate from. DOM is operationally defined as any organic matter passing through filters ranging between 0.7 and 0.2 μm in pore size, and consists of at least hundreds of thousands of individual compounds in the pico- to nanomolar concentration range (Zark et al., 2017). Based on its molecular composition, DOM can roughly be classified into chemical subgroups, some of which are indicative of its origin, and some of which furthermore have been found to preferentially interact with trace metals: For example, humic substances (i.e., polycyclic aromatic, carboxylic-rich DOM fractions) characteristic of terrestrial origin were found to form complexes with Cu and Fe in surface estuaries (Abualhaija et al., 2015). At redox interfaces and in STEs, iron(oxi)hydroxide precipitation in the STE immobilized specific "humic-like", terrestrial vascular plant-derived DOM fractions (Riedel et al., 2013, Seidel et al., 2015, Linkhorst et al., 2017, Sirois et al., 2018). In surface estuaries, organically complexed Fe and Cu were proposed to undergo ligand exchange from large, colloidal humic-terrestrial to small, marine ligands, along the salinity gradient (Batchelli et al., 2010, Muller and Batchelli, 2013). Therefore, co-variations of specific DOM molecules, and Cu and Fe abundances may indicate shared provenance (marine *vs.* terrestrial) as well as direct interaction (i.e., complex formation).

To investigate the molecular composition of DOM, ultra-high-resolution Fourier transform ion cyclotron resonance mass spectrometry (FT-ICR-MS), allows the simultaneous detection of tens of thousands of compounds in solid-phase extracted natural DOM samples (Riedel et al., 2013, Seidel et al., 2015, Linkhorst et al., 2017). Furthermore, the high mass resolution enables the assignment of elemental formulae, which in turn are proxies for structural and chemical properties of the detected compounds (Koch and Dittmar, 2006, 2016, Seidel et al., 2014, 2015). While DOM molecular fingerprinting of specific aqueous environments is a now well-established technique, the investigation of mobile, soluble metal-DOM complexes on a molecular

level using FT-ICR-MS is still in its pioneering stage. Data on newly described complexes are limited to only few regions and sample types, and only a few (2–3 molecular formulae) have been reported in each publication (e.g. Waska et al., 2015, Boiteau et al., 2016, Chen et al., 2016). However, such data are crucial in understanding direct DOM-metal interactions (rather than observed co-variations), because the chemistry of these ligands determines the stability and solubility of metal-DOM complexes in aqueous environments. Ultimately, this information is a requirement for the groundtruthing of reactive transport models to assess and predict geochemical dynamics across ecohydrological gradients (Turner et al., 2016).

In our study, we therefore set out to investigate the organic and inorganic speciation of two selected trace metals, Cu and Fe, in two exemplary STEs on Spiekeroog, a barrier island in the German Wadden Sea. The groundwater-seawater interactions on several Spiekeroog beach locations have been studied in the past (Röper et al., 2012, Röper et al., 2014, Reckhardt et al., 2015, Seidel et al., 2015, Beck et al., 2017), and we designed targeted campaigns based on these data to acquire a high sample diversity from different biogeochemical conditions within the STEs. The rationale for choosing Fe and Cu lies within their high bioavailability and ecological relevance as micronutrients, as well as their ability to form stable complexes with natural organic ligands (van den Berg, 1984, Rue and Bruland, 1995). We were particularly interested in finding correlative links between the metals' speciation and co-occurring DOM, and how they might co-evolve through different geochemical zones typically found in STEs. In addition, we aimed at identifying intact, mobile Fe- and Cu- complexes in DOM to elucidate their molecular properties, and find clues on their origins and fate within the STE and beyond.

For these purposes, we collected groundwater, groundwater seepage, and seawater from two STEs at the West and South coast of Spiekeroog Island. We applied a novel sample processing combination which includes in situ speciation (ferrozine method for Fe(II) determinations), size fractionation (0.2 μm and 0.02 μm syringe filtration), Cu-ligand titration using competitive ligand equilibration-adsorptive cathodic stripping voltammetry (CLE-ACSV), and chemical fractionation and molecular characterization through sequential SPE and subsequent ultra-high-resolution FT-ICR-MS analyses of the yielded extracts.

2. MATERIALS AND METHODS

2.1. Study sites

Spiekeroog Island belongs to the East Frisian island chain in the German North Sea, bordering the Wadden Sea to the South and the open ocean to the North (Fig. 1). The island consists mainly of fine-to coarse-grained Holocene sands atop Pleistocene and Pliocene sand deposits, which are intersected by a clay layer at 44–55 meters below sea level (mbsl) depth. The clay layer underlies the precipitation-fed freshwater lens, which reaches a maximum thickness of 40 mbsl along the western dune belt of the island (Röper et al., 2012). Between the Holocene and Pleistocene sediment layers, Spiekeroog contains peat lenses, approximately 6–7 ka old, which stem from several successions of sea-level rise. Hydrolysis of these peat lenses by percolating groundwater causes locally restricted enrichment of the groundwater with humic-rich DOM and associated trace elements (Streif, 2002, Seibert et al., 2018).

Despite its comparatively simple geology and small size (~21 km^2), the island consists of a variety of coastal environments, with extensive salt marshes at the southern coast, high-energy beaches along the northern shorelines, and sheltered low-energy beach sites to the south-west, which host the STE sites investigated in this study (Fig. 1). Spiekeroog is subject to a mesotidal regime, with average tidal amplitude of 2.7 m. The STE on site "South Beach" (SB), which faces the Wadden Sea and extends over ~150 m width during low tide, has three hydrologically and biogeochemically distinct zones along the salinity gradient (Reckhardt et al., 2015, Seidel et al., 2015): An oxic, fresh meteoric groundwater zone is located above the high-water line near the dune belt, with salinities below 5 and nitrate concentrations up to ~200 μM. A salinity transition zone (~15–17) marks the infiltration area of the tidal recirculation cell and the upper boundary of the upper saline plume (USP). It is located approximately midway between dune base and low-water line, and has elevated pore water concentrations of dissolved organic carbon (DOC, 200–250 μM) and Fe (up to 80 μM) indicating high microbial respiration rates, probably accelerated by marine organic matter (OM) infiltration during high tide. The low tide water line marks the lower boundary of the USP and is the exfiltration zone of brackish groundwater. It is characterized by elevated levels of recirculated marine DOC, as well as a terrestrial groundwater DOM signature. The prevalence of ammonium and elevated phosphate and dissolved iron concentrations, together with evidence of moderate sulfate reduction, indicate that this zone is suboxic to anoxic. Overall, water residence times in the STE range from days to months (Reckhardt et al., 2015, Seidel et al., 2015).

Of "West Beach" (WB), the second site of this study, little is known with regards to STE biogeochemistry. Compared to SB, WB is shorter in extension (~100 m width from dune base to low-water line), and bordered seaward by a sand ridge which emerges during low tide. The intermittent runnel traps fine-grained sediments from the Wadden Sea, producing a silty-muddy layer bordering the low tide water line. On the landward side below the adjacent dune belt, the islands' fresh water lens reaches its greatest thickness (Röper et al., 2012). Discrete brackish groundwater springs have previously been detected in the vicinity of the low tide water line along WB (Röper et al., 2014).

2.2. Sampling strategy

A suite of STE pore water, seawater, and seepage water samples were collected on SB on August 28th, 2012 and on WB on November 5th, 2012 (Fig. 1). For each of the two beach sites, three STE stations were chosen along transects perpendicular to the shoreline: One station was located

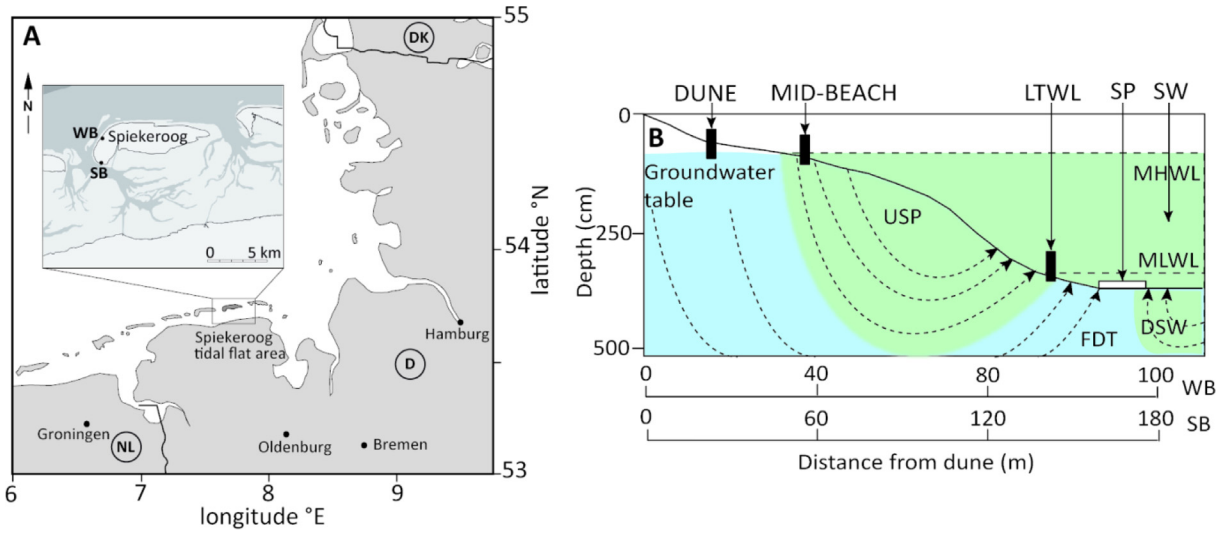

Fig. 1. (A) Map of the sampling area and location of the subterranean estuaries on Spiekeroog Island. SB = South Beach, WB = West Beach. (B) Subterranean estuary sampling scheme denoting the sampling stations. DUNE = station at the dune base, MID-BEACH = station between dune and low tide water line, LTWL = station at the low tide water line, SP = seepage meter, SW = seawater sampling site (during high tide). MHWL = Mean high water line, MLWL = Mean low water line. The subterranean estuary encompasses a USP = Upper saline plume (tidal seawater recirculation cell), FDT = fresh groundwater discharge tube, and a DSW = deep saline wedge. Schematic diagram of beach topography and STE zonation is based on geochemical data and numerical models from Seidel et al. (2015) for South Beach.

close to the dunes (approximately 20 m seaward from the marram grass belt, hereafter referred to as "dune"), one station at the low tide water line ("LTWL" = low tide water line), and one station approximately halfway between the other two ("mid-beach"). At each of the stations, stainless steel push-point samplers were inserted at three depths below the sediment surface: 50 cm, 100 cm, 150 cm (Reckhardt et al., 2015, Seidel et al., 2015). After flushing the samplers with pore water using polyethylene (PE) syringes, subsamples were collected for salinity, pH, and temperature measurements. Thereafter, approximately 2 L of pore water were transferred into Nalgene polycarbonate bottles *via* an in-situ vacuum filtration setup. To minimize contamination with atmospheric oxygen, the polycarbonate (PC) bottles were equipped with vacuum caps with polycarbonate stopcocks on in- and outlets. The bottles were flushed and filled to a slight overpressure high-purity argon (Ar) gas (Alphagaz, AirLiquide) in the laboratory in the morning before the campaign. Furthermore, the push-point samplers and in-line filter cartridges (Whatman Polycap TC 36) were pre-flushed with aliquots of the pore water sample using syringes, and attached to the vacuum caps of the PC bottles pre-filled with fresh sample solution. Thereafter, the vacuum was applied to the PC bottles to induce water flow. Immediately after the desired volume (~2 L) had been collected, a small Ar gas bottle was attached to the vacuum outlet to create an overpressure. Subsamples were then collected in situ from the vacuum pore water inlet. The Fe(II) samples were processed first by pipetting 1 mL into 2 mL Eppendorff safe-lock PP tubes pre-filled with 100 µL ferrozine solution (Viollier et al., 2000). Then, subsamples for Cu ligand titrations, and dissolved nutrient, trace metal, and DOC determinations were collected. One set of subsamples was filtered additionally through 0.02 µm Whatman Anotop syringe filters for the determination of soluble trace metals. The 0.2 µm and 0.02 µm filtered fractions will hereafter be referred to as "total dissolved" and "soluble" fraction, respectively, with a "colloidal" fraction yielded between 0.2 µm and 0.02 µm. The whole in situ sample collection procedure, including extraction of subsamples from the main bottle, took approximately one hour per sample. Because sample collection and subsample extraction was done in Ar-flushed bottles and tubings, artifacts from oxygen contaminations were likely negligible.

In addition to the pore water samples from the STEs, seawater samples were taken with acid-washed 2 L Nalgene PC bottles. Finally, SGD was collected by deploying cylindrical, Lee-type (Lee, 1977) PE seepage meters (67 cm diameter, 15 cm height) equipped with a 12 mm outlet connected to an acid-washed 3 L bag-in-box PE bag, in the surf zone approximately 3–5 m below the low tide water line, for the duration of the sampling campaign (~5–6 h). Both seawater and seepage water samples were stored in a cool box and filtered upon return to the laboratory. There, subsamples were taken for Cu ligand titrations, and dissolved and soluble nutrient, trace metal, and DOC determinations.

All sampling and sample storage equipment consisted of hard plastics such as PE, polypropylene (PP), PC, fluorinated high-density polyethylene (HDPE), and polytetrafluoroethylene (PTFE), with the exception of the low-density PE seepage bags, and the pre-combusted 20 mL glass vials for storage of DOC samples ("total dissolved" fraction). Flexible tubing and fittings for the vacuum caps were made of viton, a fluorinated, chemically inert elastomer. The casing and filter material of the filter cartridges consisted of PP and PES (polyethersulfone), respectively. All plastics sampling materials were soaked in a series of acids diluted with

ultrapure water (2% HNO_3 p.a., overnight at 50 °C, 0.01 M HCl suprapur, several weeks), with at least 5 rinses of ultrapure water between each acid soaking step.

2.3. Sample processing

The subsamples for trace metals and DOC analyses were acidified to pH = 2 with HCl suprapur immediately after return to the laboratory. Subsamples collected for Fe(II), trace metals, and DOC and total dissolved nitrogen (TDN) analyses were stored in the dark at 4 °C. Nutrient and Cu titration subsamples were stored frozen (−20 °C) until analyses.

The large-volume samples were solid-phase extracted (SPE) in two steps (Fig. 2) over pre-cleaned 500 mg Waters Oasis HLB sorbents. SPE is routinely used to preconcentrate and desalinate DOM from natural waters for FT-ICR-MS analyses (Dittmar et al., 2008). We modified a two-step SPE from Waska et al. (2015), which aimed at the collection of chemically distinct DOM- and metal-DOM fractions (Fig. 2). In brief, in the first step of the SPE, samples were extracted at their natural pH to isolate intact, neutral to weak acidic metal-DOM and DOM compounds (NWA fraction). Then, permeates from the first extraction step were acidified to pH = 2 and passed through the cartridges once more, to isolate free basic and strong acidic ligands, and strongly complexed basic and acidic metal-DOM compounds (BSA fraction). In addition to the pre-cleaning procedure of the cartridges described in Waska et al. (2015), the pH-adjusted ultrapure water used to rinse the cartridges was de-aerated by bubbling it with Ar gas. For the pH adjustments of samples and ultrapure rinsing water, suprapur HCl and NaOH were used. A sequential elution of Fisher Optima grade methanol, Aristar trace metal grade acetone, and ultrapure water (4 mL each) was applied to elute the NWA and BSA fractions from the SPE sorbents. All fractions were stored in acid-washed, solvent-conditioned PTFE-coated Zinsser vials. A set of subsamples was transferred into acid-washed PFA autosampler vials (AHF Germany), evaporated to dryness at 50 °C, and picked up in ultrapure water acidified with 2% HNO_3 suprapur, to determine extraction efficiencies of organically bound Fe and Cu. The acidic subsamples were stored at 4 °C, and all SPE-extracts were stored at −20 °C.

2.4. Sample analyses

Dissolved nutrients (nitrate, nitrite, and ammonium) were measured spectrophotometrically based on

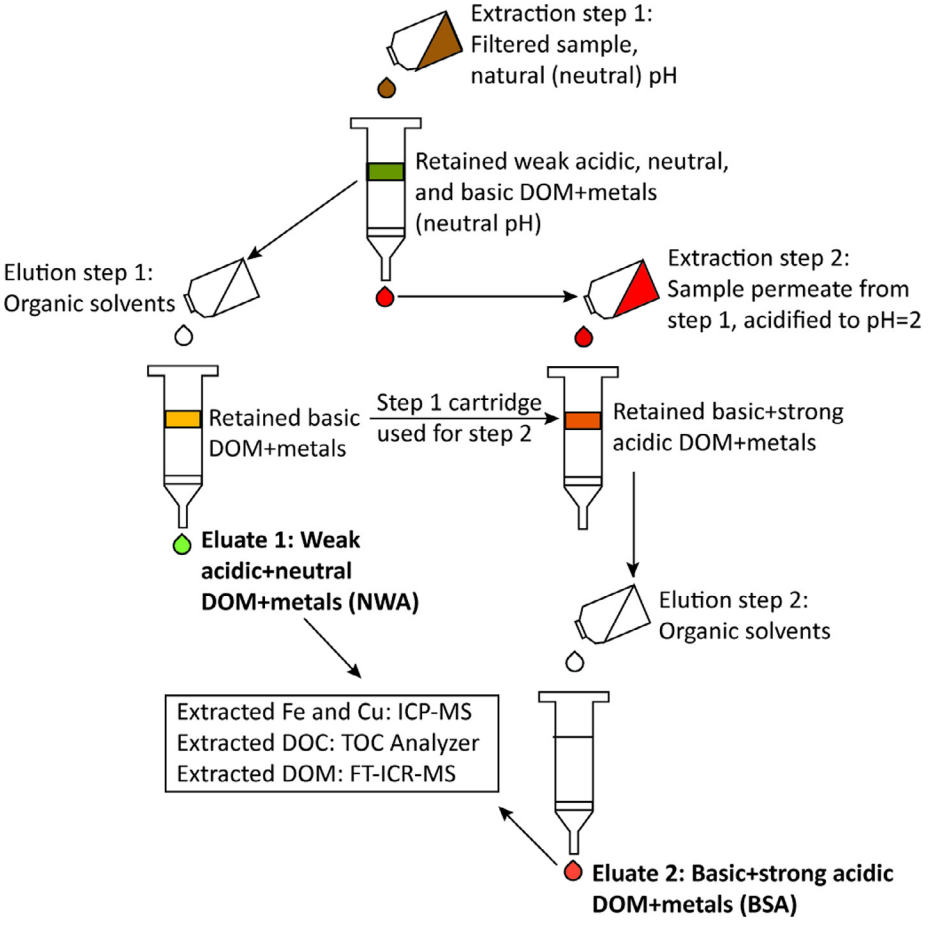

Fig. 2. Schematic diagram of the sequential extraction-elution setup.

Reckhardt et al. (2015), with an analytical error of <10%. DOC and TDN were measured on a Shimadzu TOC-VCPH using a deep sea Atlantic seawater reference material for trueness (Hansell Lab, Florida, USA). The accuracy was better than 5%. DON concentrations were calculated by subtracting the sum of the inorganic nitrogen species (ammonium, nitrate, and nitrite) from TDN concentrations.

Concentrations of Fe and Cu in all natural water samples (0.2 µm and 0.02 µm filtered) and extract subsamples were measured via inductively coupled plasma mass spectrometry (HR-ICP-MS, Thermo Element 2) at a resolution of R = 4500 together with a CASS-5 coastal seawater reference material (National Research Council of Canada, NRC) with an accuracy of better than 5% for the two elements. The samples were spiked with an yttrium internal standard to correct for instrument drift and matrix effects. Once the concentrations of Cu and Fe were known in both the solid-phase extracts and the natural aqueous samples, we calculated the (solid-phase) extraction efficiencies as Met(ex)/Met(aq) * 100.

Fe(II) was measured spectrophotometrically through absorbance at 562 nm using a method adapted from Viollier et al. (2000). Calibration solutions were made of dilutions of Fe(II)Cl_2 salt solution in de-aerated ultrapure water in the range of 5–100 µM. No reduction step was included to determine Fe(III) concentrations in the natural samples; instead, the total Fe concentrations measured by HR-ICP-MS were used for the evaluation of Fe(III) contributions.

Determinations of Cu-binding organic ligands were conducted *via* CLE-ACSV using a method modified from Buck and Bruland (2005) and Waska et al. (2015). Briefly, Cu-binding ligands of a sample are supplemented with an artificial Cu-binding chelator with known binding strengths (in our case salicylaldoxime, SA), and titrated with increasing amounts of a Cu spike until all natural ligand binding sites become saturated. Excess and weakly bound Cu is then measured by quantitative adsorption-desorption of the electroactive Cu-SA complex to and from the mercury electrode. For the analysis, 10 mL subsamples were equilibrated in 15 mL PTFE cups, each with increasing amounts of Cu concentrations (generally in the range of 0–150 nM) in the presence of a HEPES buffer to stabilize the sample at pH = 7.8. For Cu additions, HCl-diluted National Institute of Standards and Technology (NIST) traceable standard stock solutions were used. After two hours of equilibration, 2 µM of SA were added to the titration series. The equilibration times of two hours for natural ligands with Cu, and an additional hour with SA, are deemed sufficient for complete equilibration as demonstrated by thorough tests provided by Buck and Bruland (2005) for water samples from a similar coastal environment along a salinity gradient. This was recently confirmed by an intercomparison experiment (Buck et al., 2012). The samples were then equilibrated for another hour and subsequently measured on a Metrohm 757 VA Computrace using the following parameters: Purging with nitrogen (N_2) gas for 300 s, deposition of the SA-Cu-complex at −50 mV for 60 s, scanning from −50 mV to −600 mV at a sweep rate of 20 mV s^{-1}. The resulting titration curves were further processed using an open-source metal complexation calculation program, ProMCC (Omanović et al., 2015), to yield total dissolved ligand concentrations and bulk conditional stability constants (logK's) as indicators of Cu-complex binding strength. In the program, we plugged in a suite of side-reaction coefficients customized for SA for the respective salinities of the samples. The best fits for the sample set were achieved with the Langmuir approximation, using one ligand class, and assuming complete complexation (Gerringa et al., 1995, Omanović et al., 2015).

SPE-metal-DOM samples were adjusted to 20 ppm DOC in 1:1:1 mixtures of Optima grade methanol, Aristar acetone, and ultrapure water. The samples were then filtered through 0.2 µm PTFE syringe filters into pre-washed (by acids and organic solvents) Eppendorff PP tubes, and measured on a 15 Tesla Bruker solariX XR FT-ICR-MS equipped with an electrospray ionization (ESI) source. Samples were measured in broadband ESI negative and positive ionization mode, with a flow rate of 20 µL min^{-1} and an ion accumulation time of 0.2 s. For each sample, 500 scans were acquired. An in-house deep-sea standard (North Equatorial Pacific Intermediate Water, or NEqPIW) was measured daily to control instrument drift.

2.5. Data processing

All environmental parameters, including in situ measurements of salinity, trace metal concentrations, calculated concentrations of Cu-binding ligands (CLE-ACSV) and concentrations of solid-phase-extracted organic (i.e., DOM-bound) Fe and Cu, were assembled in a metadata matrix for statistical analyses.

Calibration of the FT-ICR-MS spectra and assignment of exact molecular formulae was done using an approach modified from Seidel et al. (2014, 2015), with the addition of using isotopologue abundance patterns for metal-containing molecular formulae (McCormack et al., 2003, Boiteau et al., 2013, Waska et al., 2015, 2016). A detailed description of the method can be found in the supplementary information. The final spectra were assembled in four tables for four settings (NWA, BSA fraction, ESI negative, ESI positive mode), which also contained a rough chemical classification to DOM groups. After assigning each molecular formula in a compound group, the weighed sums of the compound groups were calculated for each individual sample mass spectrum based on the compound groups' relative signal intensities. The relative compound group contributions for each sample thus provide individual "fingerprints" of DOM biogeochemistry.

For multivariate statistical analyses, R (version 3.4.0) was used. Multivariate data analyses were performed with the package *vegan* (Oksanen et al., 2013). Prior to statistical analyses, signal intensities of the mass spectra, and environmental parameters were scaled between 0 and 1 and Hellinger transformed. Thereafter, principle coordinate analyses (PCoA) were conducted using Bray Curtis distance matrices, and environmental vectors and relative abundances of site-specific, intensity-weighed compound groups were

correlated to the PCoA scores using vegan's envfit function (999 permutations). Spearman rank tests were performed to (i) derive relationships between inorganic and organic Cu and Fe species and environmental parameters, (ii) link abundances of individual molecular formulae with Fe and Cu concentrations in the extracts, and (iii) analyze trends of detected metal-DOM formulae across environmental gradients. Only correlations with a p-value <0.05 and a correlation coefficient of >0.5 (Spearman's ρ, moderate to strong correlations) were considered in further discussions.

3. RESULTS

3.1. Fe and Cu speciation

To characterize lateral trends in the STEs, we pooled the different depth samples for each station (Table 1, Figs. 3 and 4). Distinct depth gradients were observed at the SB dune and WB LTWL sites (as indicated by the error ranges in Figs. 3 and 4), but overall, the two STEs displayed geochemically characteristic zones along the shore-perpendicular land-ocean transects.

At SB at the dune site, where salinity was lowest, DOC and TDN concentrations were highest (Table 1). They decreased towards the LTWL together with a steady increase in salinity. TDN concentrations remained low in seepage and seawater, while DOC concentrations increased slightly from the LTWL pore waters to the water column. NOx was the dominant inorganic N species in the dune site, while ammonium prevailed in the mid-beach site and at the LTWL. Dissolved organic nitrogen (DON) appeared in larger contributions from the mid-beach sites onwards into seepage and seawater (Table 1).

Parallel to DOC and TDN, Cu concentrations were highest at the SB dune site, while Fe concentrations displayed a maximum at the SB mid-beach site (Figs. 3 and 4). Cu concentrations decreased at the mid-beach site and increased again in seepage and seawater (Fig. 3A). Throughout the SB STE, Cu could be found mostly in soluble form (Cu sol), while soluble Fe (Fe sol) only dominated in stations with high Fe(II) concentrations, and was to a large part colloidal (Fe coll) in the dune site, and in seepage water and seawater (Fig. 4A–C). Cu-binding ligand (CuL) concentrations were always higher than those for total Cu and displayed similar trends with a maximum at the dune site, decreasing concentrations in mid-beach and at LTWL, and slightly elevated concentrations again in seepage and seawater (Fig. 3A). CLE-ACSV results implied that Cu was organically bound throughout the STE, and that Cu-binding ligands always occurred in excess to the total Cu concentrations. The extracted organic Cu concentrations were also significantly positively correlated with total dissolved Cu concentrations ($p < 0.001$, $\rho = 0.90$ for Cu-NWA, and $p < 0.001$, $\rho = 0.90$ for Cu-BSA). Despite this co-variance in concentrations, overall extraction efficiencies of organic Cu (as calculated based on total dissolved Cu concentrations) for both the combined NWA and BSA fractions at each of the investigated stations and depths were always below 26%, and thus at the low- to medium end of previously published data on organic Cu extraction by SPE (Mills et al., 1982, Donat et al., 1986, Waska et al., 2015). Furthermore, extraction efficiencies varied between stations and extraction setups: With the exception of the LTWL station, which had total dissolved Cu concentrations close to or below the detection limit, the extractable organic Cu-NWA fraction increased from ~ 2–10% for dune pore waters to 20–25% in seepage and seawater samples, whereas the extractable organic Cu-BSA fraction decreased slightly from ~6–9% in the dune pore waters to ~4–6% in seepage and seawater samples. In line with Cu, extractable organic Fe concentrations were also significantly positively correlated with total dissolved Fe concentrations ($p < 0.05$, $\rho = 0.65$ for Fe-NWA, and $p < 0.001$, $\rho = 0.86$ for Fe-BSA). Nevertheless, the extraction efficiencies of the organic Fe fractions (based on total dissolved Fe concentrations) were low even when NWA and BSA fractions were pooled, even lower (<15%) than those for Cu. The extracted organic Fe-NWA fraction in the SB STE pore waters was overall low at all stations (~0.01–0.7%) and sharply increased in seepage and seawater samples (~4–14%). On the other hand, the extracted organic Fe-BSA fraction was elevated at the dune station (~1.4–3%), decreased below 0.5% at mid-beach and LTWL stations where Fe(II) concentrations were at their highest, and increased slightly again in seepage and seawater (~0.6–2%).

Table 1
Geochemical characteristics of the Spiekeroog STE. Values are measured ranges for the different sampling depths (50–150 cm). SB = South Beach, WB = West Beach, LTWL = Low tide water line, SP = seepage water, SW = sea water. NOx = sum of nitrate and nitrite. b.d. = below detection limit. *Salinity was measured only in one of the two samples.

Station	Salinity	DOC (μM)	TDN (μM)	NH_4^+ (μM)	NOx (μM)	DON (μM)	Cu (nM)	Fe (nM)	Mn (nM)
SB Dune	0.38–0.96	142–443	14.1–443	b.d.–3.88	0.63–468	b.d.–13.7	5.19–87.0	17.7–1054	11.7–57.0
SB Mid Beach	17.6–19.2	164–181	27.4–55.3	14.3–42.1	b.d.–1.02	9.29–18.5	0.91–2.02	15982–33888	1565–3051
SB LTWL	24.3–28.6	125–175	16.7–36.0	10.8–26.6	b.d.–0.13	5.86–9.21	b.d.–0.68	257–503	2592–4279
SB SP	32.0–32.1	182–198	13.5–14.5	b.d.–1.04	0.09–0.13	12.3–14.4	13.1.–13.8	9.86–11.1	255–260
SB SW	31.7–32.2	158–163	18.3–30.9	b.d.–0.14	3.93–23.8	6.94–14.4	8.34–9.33	10.9–17.7	15.3–17.2
WB Dune	17.2–19.7	88.6–120	86.4–113	b.d.–1.01	37.8–77.2	8.26–75.5	29.2–57.3	2.51–26.1	6.84–42.8
WB Mid Beach	27.1–27.9	103–118	45.8–69.8	b.d.–1.67	50.2–66.9	b.d.–2.37	18.1–18.4	8.11–22.8	16.0–8450
WB LTWL	16.3–27.2	147–346	21.1–26.9	7.31–14.0	b.d.	11.0–14.1	103–397	7122–26,896	489–1001
WB SP	31.0*	166–177	34.1–40.7	b.d.–12.8	8.63–9.08	12.4–25.2	16.5–18.0	13.0–15.3	373–424
WB SW	30.4–31.0	165–173	33.8–34.3	b.d.–3.44	b.d.–8.09	26.6–40.7	19.2–19.7	14.2–18.2	66.6–73.2

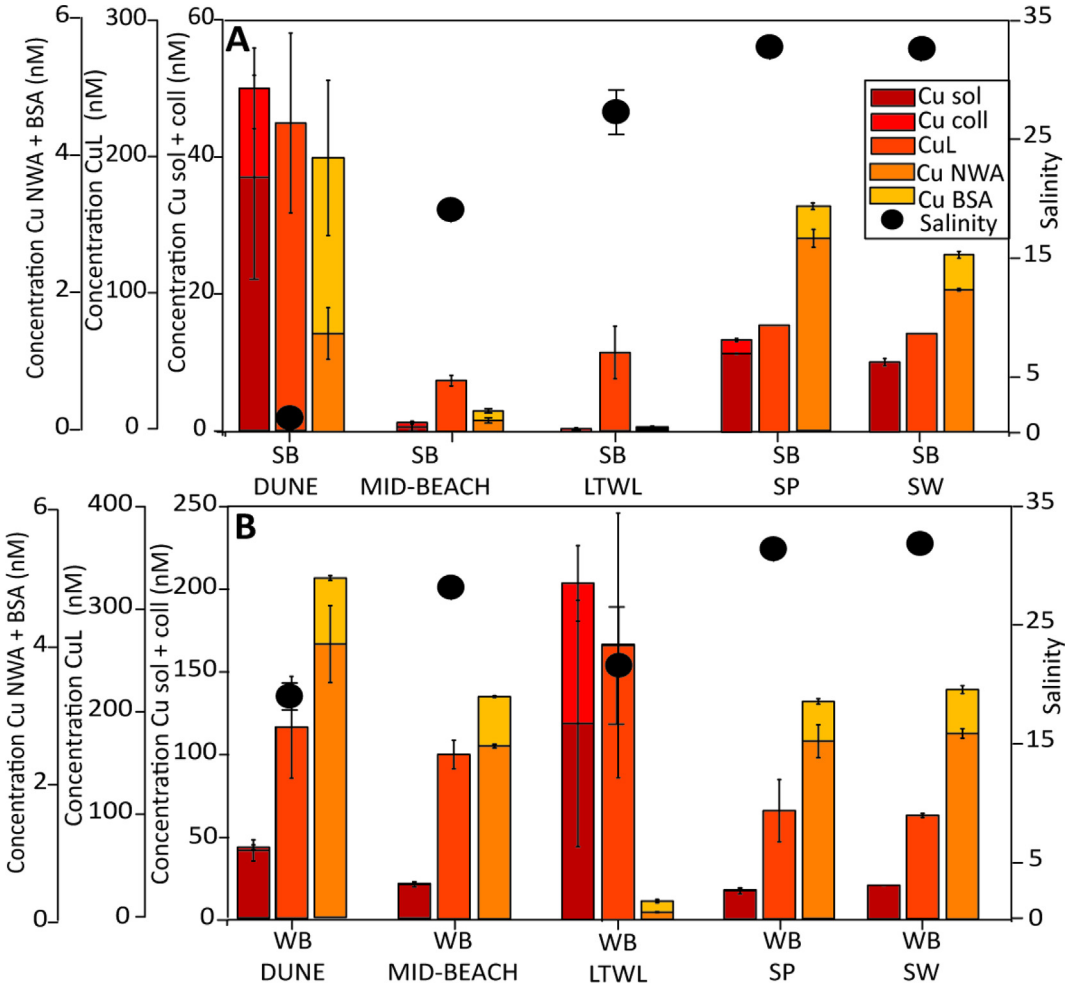

Fig. 3. Inorganic and organic Cu species in ground- and seawater samples of the (A) SB and (B) WB STEs. SB = South Beach, WB = West Beach, LTWL = Low tide water line, SP = seepage water, SW = sea water. Cu sol = soluble Cu (<0.02 μm), Cu coll = colloidal Cu (<0.2 μm, >0.02 μm), CuL = Cu-binding ligands (CLE-ACSV), Cu NWA = NWA fraction of extractable organic Cu, Cu BSA = BSA fraction of extractable organic Cu. Error bars denote standard errors of means for the pooled sampling depths (50, 100, and 150 cm). Note different scales for Cu concentrations in aqueous samples, Cu ligand concentrations (from voltammetry), and extracted organic Cu-NWA and Cu-BSA fractions.

In contrast to SB, at WB, dune site pore waters were already brackish, and while salinity increased toward the mid-beach and in seepage and seawater, it showed a marked decrease in pore water at the LTWL (Table 1, Fig. 3B and 4D–F). Furthermore, DOC concentrations were also highest at the LTWL. The overall TDN concentrations decreased from land to ocean, like those at SB. NOx were the prevailing N species in dune and mid-beach samples, with a change to ammonium at the LTWL and in seepage and seawater (Table 1). At WB, Fe and Cu concentrations displayed their maxima at the LTWL site, with Cu concentrations three- to fourfold higher, compared to those at the SB and WB dune sites, respectively (Fig. 3). While at SB, maxima in total Fe concentrations occurred in tandem with maxima in Fe(II) and soluble Fe concentrations, the maxima of total Fe concentrations at WB LTWL were comprised of high Fe(II), and at the same time, high colloidal Fe concentrations (Fig. 4D). Similar to SB, CLE-ACSV results indicated that most Cu was organically complexed and that Cu-binding ligands occurred in excess to total dissolved Cu concentrations throughout the WB STE. In contrast to SB, extractable organic Cu concentrations did not show any correlations with total Cu concentrations. In addition, organic Cu extraction efficiencies were lower at WB (<18%) than at SB (<26%) for all of the extracted fractions. Both, extracted organic Cu-NWA and Cu-BSA fractions, increased with increasing salinity, from the dune station (~9–11% for Cu-NWA and ~2–3% for Cu-BSA) to seepage and seawater (~13–17% for Cu-NWA and ~3–4% for Cu-BSA). Extractable organic Fe-NWA concentrations were significantly positively correlated with total dissolved Fe concentrations ($p < 0.05$, $\rho = 0.66$), whereas no correlations could be found for Fe-BSA concentrations with those of total dissolved Fe. Analogous to Cu, both the extraction efficiencies of organic Fe-NWA and Fe-BSA increased with increasing salinity,

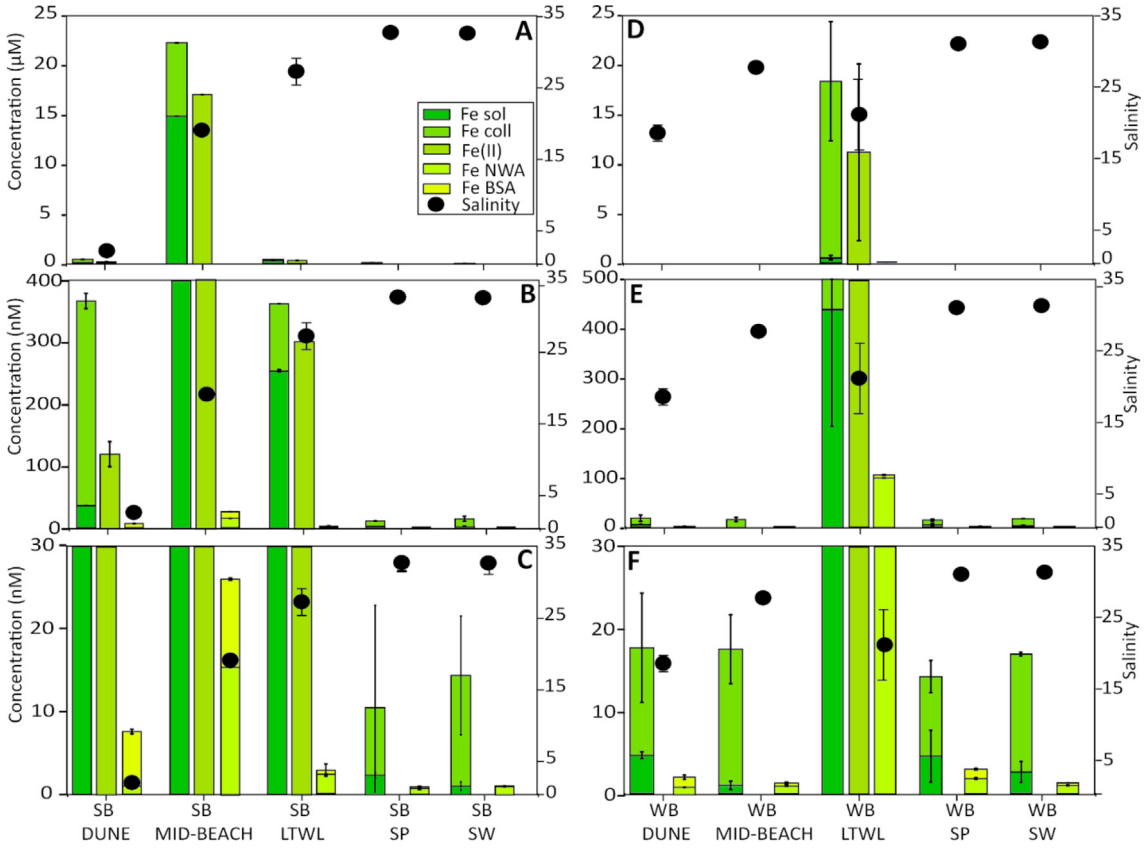

Fig. 4. Inorganic and organic Fe species in ground- and seawater samples of the (A-C) SB and (D-F) WB STEs. SB = South Beach, WB = West Beach, LTWL = Low tide water line, SP = seepage water, SW = sea water. Fe sol = soluble Fe (<0.02 µm), Fe coll = colloidal Fe (<0.2 µm, >0.02 µm), Fe(II) = reduced Fe(II) (ferrozine method), Fe NWA = NWA fraction of extractable organic Fe, Fe BSA = BSA fraction of extractable organic Fe. Error bars denote standard errors of means for the pooled sampling depths (50, 100, and 150 cm). From top-down, scales are enhanced (zoomed in) to display compositions of low-concentration fractions. The left y axes show concentrations, the right y axes show salinities.

from the dune station (~4–5% for Fe-NWA and ~2–3% for Fe-BSA) to seepage and seawater (~5–15% for Fe-NWA and ~2–11% for Fe-BSA).

3.2. Molecular characteristics of SPE-DOM

In ESI negative mode, the NWA fraction of all samples (all SB and WB stations, and all depths) combined yielded a total of 18,674 unambiguous molecular formulae, and in positive mode a total of 19,663. In comparison, the BSA fraction had a larger number of detected molecular formulae: For the same adjusted DOC concentrations as the NWA fraction, the BSA fraction samples yielded totals of 29,770 and 21,206 unambiguous molecular formulae in ESI negative and positive mode, respectively. When calculating the intensity-weighed sums of the compound classes for all SB and WB stations at all depths combined (Fig. S1A), the four different analytical settings showed trends which persisted even amongst geochemically different zones of the STEs: N-containing aliphatic and oxygen-poor unsaturated aliphatic compounds were more abundant in the NWA fractions, while polyphenols and highly unsaturated, oxygen-rich compounds had relatively higher contributions in the BSA fractions. ESI positive mode furthermore appeared to favor the detection of N-containing aliphatic compounds and oxygen-poor polyphenols in both, NWA and BSA fractions, of all measured samples combined (Fig. S1A). Differences between the extracted DOM fractions and their respective measurement modes overall appeared to have a larger effect on DOM composition than the differences between sampling sites. For example, when conducting PCoAs using both, NWA and BSA fractions, measured in the same ionization mode, we found that samples were primarily grouped by the two extracted fractions, which masked patterns based on environmental conditions and STE biogeochemistry. However, within the analytical window of each setup (extraction and ionization), molecular composition displayed site-specific characteristics, for example changes along the salinity gradients of both STEs, as demonstrated in Fig. S1B–E for each fraction measured in ESI negative and positive mode. Therefore, in the following results and discussions sections, we focus on site-based characteristics for each

DOM fraction and ionization mode (ESI neg NWA, ESI neg BSA, ESI pos NWA, ESI pos BSA) separately.

3.3. SPE-DOM characteristics and associated environmental factors

Fig. S2 displays all samples (SB, WB, dune to seawater) from all depths based on their position along principle coordinates 1 (x-axis) and 2 (y-axis) for the four analytical settings (ESI negative, ESI positive, NWA, BSA). Environmental parameters which correlate with any of the two axes with a $p < 0.05$, and chemical compound group proportions with a $p < 0.001$ are also displayed as blue and red arrows, respectively. Salinity was always associated with SPE-DOM compound class characteristics, regardless of the analytical setting, either along PC1 (Fig. S2B–D), or PC2 (Fig. S2A). Along this environmental gradient, sites were grouped in the order SB dune => WB dune, SB and WB mid beach, SB and WB LTWL => SB and WB seepage and seawater. A second major predictor of molecular composition was STE location (e.g., SB *vs.* WB). Patterns in relative compound class contributions were correlated to salinity, in that unsaturated aliphatics and N-containing aliphatics were more abundant in seepage and seawater samples, whereas polyphenols and polycyclic aromates (PCAs) were predominantly found in the SB dune samples with the lowest salinities. In addition, WB samples were characterized by higher DOM masses (as indicated by NM, or nominal mass), and had higher amounts of heteroatoms (N, S, P) compared to SB samples (Fig. S2A and B).

The NWA samples measured in ESI positive mode (Fig. S2B) were exceptional compared to the other analytical settings: Although salinity (PC1, 35% explained distribution) was clearly a main driver here as well, STE location had a relatively higher impact (PC2, 26% explained distribution). Furthermore, the highest abundances of polyphenols and polycyclic aromates were found in WB LTWL and seawater samples, whereas in all of the other analytical settings, these aromatic compound classes were associated with low-salinity samples, for example at the SB dune site. As a result, the relative abundance of the polyphenol compound class was consistently negatively correlated with salinity across all analytical settings and for both SB and WB ($p < 0.05$ or less, $\rho = -0.54$ to -0.91), but not for the NWA fraction at WB STE measured in ESI positive mode.

To examine spatial trends in organic Cu and Fe extractability, extracted organic Cu and Fe are displayed as environmental parameters (blue arrows and names) in Fig. S2. The concentrations of extracted Cu-NWA were positively correlated with salinity in the NWA samples (Fig. S2A and B), while the concentrations of extracted Cu-BSA and Fe-BSA, were negatively correlated with salinity in the BSA samples, and associated with high polyphenol abundances at the SB dune site (Fig. S2C and D).

3.4. Links between extracted organic Fe and Cu concentrations and DOM molecular properties

Spearman rank tests were performed to explore correlations between the concentrations of extracted organic Cu and Fe with the relative abundances of individual molecular formulae for SB and WB separately. Such correlations may be indicative of Cu- and Fe-containing complexes (Waska et al., 2016). O/C ratios of molecular formulae showing significant positive correlations with extracted Cu and Fe ($p < 0.05$, $\rho > 0.5$) were displayed against their H/C ratios in van Krevelen plots to evaluate trends in chemical characteristics (Figs. 5 and 6). Extracted Cu concentrations of the NWA fractions correlated with 2090 and 1670 molecular formulae in negative and positive mode, respectively, and extracted Cu-BSA concentrations correlated with 4665 and 2445 molecular formulae in negative and positive mode, respectively (Fig. 5). In comparison, organic Fe concentrations in the NWA extracts correlated positively with 1162 and 250 molecular formulae in negative and positive mode, respectively, while in BSA extracts, organic Fe concentrations correlated positively with 5306 and 2090 molecular formulae in negative and positive ionization mode, respectively (Fig. 6). Overall, NWA fractions correlating with extracted organic Cu and Fe were characterized by elevated H/C ratios and decreased O/C ratios compared to BSA fractions, indicating a prevalence of aliphatics in the former compared to more aromatic compounds in the latter fractions. For the NWA fractions, this trend was even more pronounced in ESI positive mode compared to ESI negative mode; for the BSA fractions, the H/C and O/C ratios did not change substantially with different ionization modes (Fig. 5 and 6).

3.5. Characteristics of identified metal-DOM complexes

In ESI negative mode, 37 masses in the NWA fraction, and 215 masses in the BSA fraction displayed $^{63/65}$Cu isotopologue patterns in at least three samples. Unambiguous Cu-containing molecular formulae could be assigned to none of the masses in the NWA fraction, and 7 in the BSA fraction. In ESI positive mode, 186 and 23 masses in the NWA and BSA fractions, respectively, had $^{63/65}$Cu isotopologue patterns in at least three samples, and for 54 in the NWA fraction and 5 in the BSA fraction, unambiguous Cu-containing formulae were found (Tables 2 and 3). The discrepancy between numbers of detected isotopologues and final unambiguous molecular formulae was primarily the result of the conservative knock-out criteria. For example, in ESI negative mode of the NWA samples, molecular formulae were assigned to 33 out of the 37 masses with reproducible isotopologue patterns. Of those, 4 were unambiguous non-Cu containing formulae and 7 were unambiguous Cu-containing formulae. The remaining 22 consisted of multiple Cu-containing, together with unambiguous non-Cu-containing formula assignments, in which case preference was given to the latter (step 5 of knock-out criteria). In total, 66 unambiguous Cu-DOM compounds could be identified in all analytical settings, with an average "assignment rate" of ~25% for masses with detectable reproducible ($n \geq 3$) isotopologues (Tables 2 and 3, Figs. 5 and 6). Most of the Cu-containing formulae were complexes with Cu(II); only two of the detected formulae were with Cu(I). With one exception, all of the identified complexes contained at least one N atom.

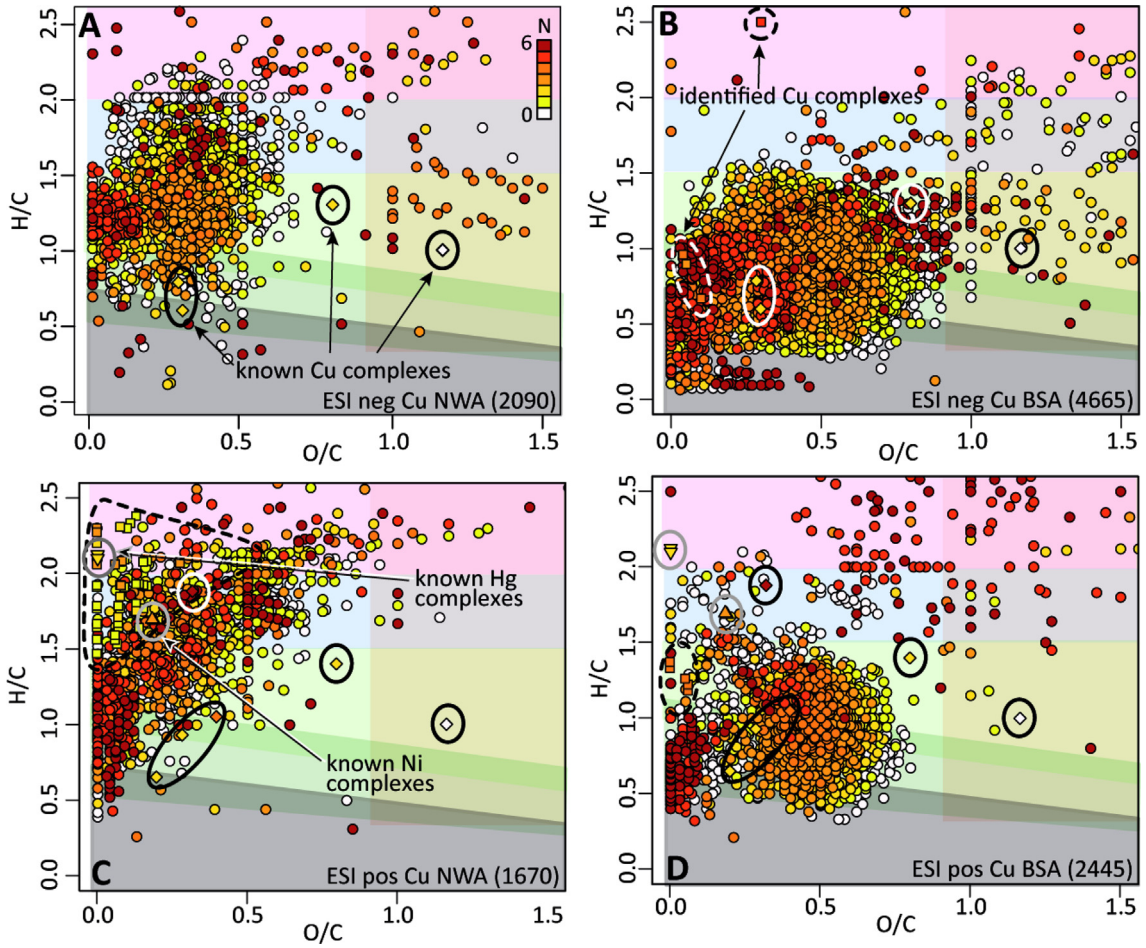

Fig. 5. Van Krevelen plots showing the O/C (x axes) and H/C (y axes) ratios of Cu-correlated and Cu-binding molecular formulae from all collected samples (both STEs) in the four analytical settings. Numbers next to the analytical settings denote amounts of non-Cu containing molecular formulae showing a significant positive correlation with extractable organic Cu (Spearman, $p < 0.05$, $\rho > 0.5$). Circles denote non-Cu containing formulae which are positively correlated with extracted organic Cu concentrations, squares denote unique Cu-containing formulae, diamonds denote formulae of known Cu-containing complexes, and triangles denote formulae of known organic complexes with other metals, Ni and Hg, as described in the literature (Tables 2 and 3). The color scale of the circles displays N contents of the formulae. The color scale of the van Krevelen space indicates DOM compound classes, with increasing H/C ratio (y-axis): Grey = polycyclic aromates, dark green = polyphenols, light green = highly unsaturated compounds, blue = unsaturated aliphatics (which may contain peptides when N is present), pink = saturated compounds with high H/C ratios which can include lipids. The light brown box (O/C ratio > 0.9) denotes saturated compounds which may contain carbohydrate formulae. (For interpretation of the references to colour in this figure legend, the reader is referred to the web version of this article.)

Furthermore, the majority of Cu-containing formulae found in the NWA fraction in positive ionization mode contained one S atom. Most formulae were classified as N-containing aliphatics (peptide-like) or as saturated compounds with high H/C (lipid-like) (Tables 2 and 3). The identified complexes had overall higher H/C ratios and/or lower O/C ratios compared to the molecules which were positively correlated with extracted organic Cu concentrations (Fig. 5B–D).

In comparison with Cu, overall fewer masses were found with Fe isotopologues: In ESI negative mode, one mass in the NWA fraction and 23 masses in the BSA fraction had reproducible isotopologue patterns, whereas in ESI positive mode, no mass in the NWA fraction, and five masses in the BSA fraction had reproducible isotopologue patterns. One and five molecular formula(e) were assigned in ESI negative mode for the NWA and BSA fractions, respectively (Table 2, Fig. 6A and B). In ESI positive mode, no unambiguous, Fe-containing molecules could be identified. All formulae with Fe in ESI negative mode contained reduced Fe(II). One Fe-containing compound had a peptide molecular formula (1 in ESI neg NWA) and the others were oxygen-poor highly unsaturated compounds (5 in ESI neg BSA, Table 2).

In general, the majority of the assigned Fe- and Cu-molecular formulae were elevated in H and N, and low in O contents compared to non-metal containing formulae: For example, the (non-intensity-weighed) average formulae for Cu and Fe in the BSA fractions in ESI negative mode were $C_{14}H_{22}O_3N_5Cu(II)$ and $C_{22}H_{27}O_5N_3Fe(II)$ respec-

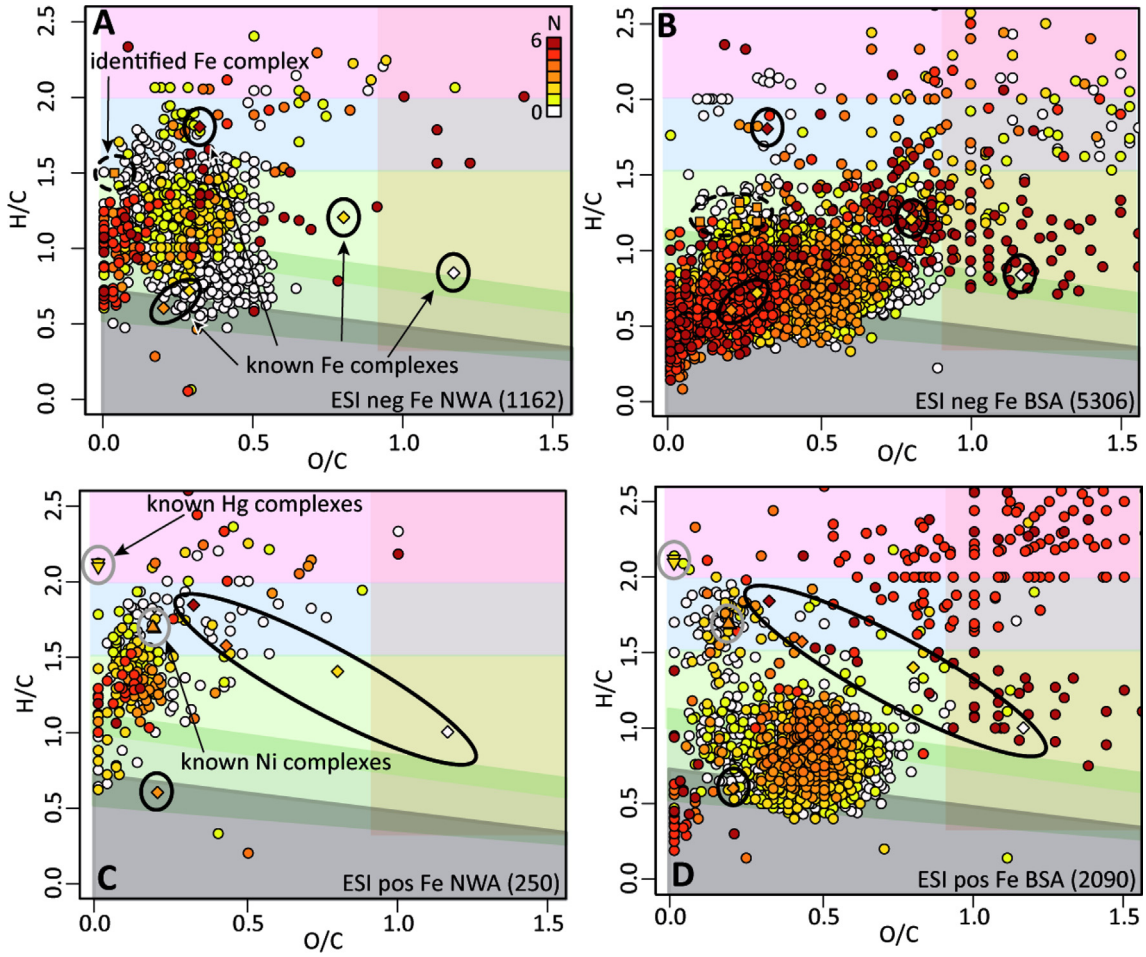

Fig. 6. Van Krevelen plots showing the O/C (x axes) and H/C (y axes) ratios of Fe-correlated and Fe-binding molecular formulae from all collected samples (both STEs) in the four analytical settings. Numbers next to the analytical settings denote amounts of non-Fe containing molecular formulae showing a significant positive correlation with extractable organic Fe (Spearman, $p < 0.05$, $\rho > 0.5$). Circles denote non-Fe containing formulae which are positively correlated with extracted organic Fe concentrations, squares denote unique Fe-containing formulae, diamonds denote formulae of known Cu-containing complexes, and triangles denote formulae of known organic complexes with other metals, Ni and Hg, as described in the literature (Tables 2 and 3). The color scale of the circles displays N contents of the formulae. The color scale of the van Krevelen space indicates DOM compound classes, with increasing H/C ratio (y-axis): Grey = polycyclic aromates, dark green = polyphenols, light green = highly unsaturated compounds, blue = unsaturated aliphatics (which may contain peptides when N is present), pink = saturated compounds with high H/C ratios which can include lipids. The light brown box (O/C ratio > 0.9) denotes saturated compounds which may contain carbohydrate formulae. (For interpretation of the references to colour in this figure legend, the reader is referred to the web version of this article.)

tively, while the average formula for the whole sample under this measurement setting was $C_{24}H_{25}O_{10}N_2$. Compared to known Cu and Fe-binding ligands such as salicylaldoxime, EDTA, and citrate, the identified compounds appeared to have lower O/C ratios. In contrast, they had compound characteristics (aliphatics containing N and S) similar to desferrioxamine B, a siderophore known to have Cu- and Fe- binding capacities (Waska et al., 2015), and to four recently reported Ni- and Hg-binding ligands isolated from natural waters (Boiteau et al., 2016, Chen et al., 2016, Figs. 5 and 6).

The artificially created metal "Me" enabled detection of isotopologues in a similar range as that for Cu (13-176). The combination of isotopologue detection and molecular formula assignment resulted in one final assignment in ESI negative mode of the NWA fraction, compared with one Fe-containing formula and no Cu-containing formulae. In ESI positive mode of the NWA fraction 5 Me-containing formulae remained compared to 54 Cu containing formulae and no Fe-containing formulae. In ESI positive mode of the BSA fraction, one Me-containing formula remained compared to five with Cu and none with Fe (Tables 2 and 3), and in ESI negative mode of the BSA fraction, no Me-containing molecular formulae remained. One formula (in ESI neg NWA) was classified as heteroatom-containing oxygen-rich saturated aliphatic, five (in ESI pos NWA) were classified as heteroatom-containing black carbon compounds with low H/C ratios (<0.200), and one (In ESI pos BSA) was classified as oxygen-poor polyphenol. In total, seven "false positive", Me-containing formulae remained

Table 2
Detected Fe- and Cu-DOM complexes in negative ionization mode, in comparison with reported complexes from known ligands (citrate, salicylaldoxime, EDTA, 1, 2-nitroso-naphthol, desferrioxamine B). Ligand data from Waska et al. (2015)** and Waska et al. (2016)*. NWA = neutral & weak acidic fraction, BSA = basic & strong acidic fraction. Compound groups are: unsat. + N = unsaturated aliphatic compounds with N; sat. O/C-NSP = saturated compounds with high O/C and N, S or P; sat. H/C-NSP = saturated compounds with high H/C and N, S or P; BC-NSP = black sat. O/Cn-like with N, S or P; O-poor poly = Oxygen-poor polyphenol-like; O-poor h. unsat. = Oxygen-poor highly unsaturated compounds; O-rich h. unsat. = Oxygen-rich highly unsaturated compounds.

Sample	m/z	Molecular formula	H/C	O/C	Compound group
NWA	464.2371	$C_{26}H_{38}ON_3Fe(II)^-$	1.500	0.038	unsat. + N
	551.3208	$C_{10}H_3O_{17}N_5PMe^-$	0.400	1.700	sat. O/C-NSP
BSA	313.0816	$C_8H_{20}O_4N_5Cu(II)^-$	2.625	0.500	sat. H/C-NSP
	315.0972	$C_8H_{22}O_4N_5Cu(II)^-$	2.875	0.500	sat. H/C-NSP
	325.1179	$C_{10}H_{24}O_3N_5Cu(II)^-$	2.500	0.300	sat. H/C-NSP
	329.1128	$C_9H_{24}O_4N_5Cu(II)^-$	2.778	0.444	sat. H/C-NSP
	416.0340	$C_{21}H_{13}O_2N_4Cu(II)^-$	0.667	0.095	BC-NSP
	458.1174	$C_{25}H_{23}ON_4Cu(II)^-$	0.960	0.040	O-poor poly
	639.1952	$C_{39}H_{35}O_2N_3Cu(II)^-$	0.897	0.051	O-poor poly
	406.1224	$C_{21}H_{24}O_2N_3Fe(II)^-$	1.190	0.095	O-poor h. unsat.
	470.1021	$C_{21}H_{24}O_6N_3Fe(II)^-$	1.190	0.286	O-poor h. unsat.
	470.1384	$C_{22}H_{28}O_5N_3Fe(II)^-$	1.318	0.227	O-poor h. unsat.
	472.1177	$C_{21}H_{26}O_6N_3Fe(II)^-$	1.286	0.286	O-poor h. unsat.
	480.1228	$C_{23}H_{26}O_5N_3Fe(II)^-$	1.174	0.217	O-poor h. unsat.
Ligands	279.9078	$C_6H_5O_7ClFe(III)^-$	0.833	1.167	sat. O/C*
	465.9427	$C_{12}H_{12}O_{14}NaCu(II)^-$	1.000	1.167	sat. O/C*
	325.9996	$C_{14}H_{10}O_4N_2Fe(III)^-$	0.714	0.286	BC-NSP*
	334.0021	$C_{14}H_{11}O_4N_2Cu(II)^-$	0.786	0.286	O-poor poly*
	343.9948	$C_{10}H_{12}O_8N_2Fe(III)^-$	1.200	0.800	O-rich h. unsat.*
	351.9973	$C_{10}H_{13}O_8N_2Cu(II)^-$	1.300	0.800	O-rich h. unsat.*
	407.0099	$C_{20}H_{12}O_6N_2Cu(I)^-$	0.600	0.200	BC-NSP*
	572.0551	$C_{30}H_{18}O_6N_3Fe(II)^-$	0.600	0.200	BC-NSP*
	648.2343	$C_{25}H_{45}O_8N_6ClFe(II)^-$	1.800	0.320	unsat. + N **

in the dataset. Six of these seven formulae contained P, which was absent in any of the identified Cu- and Fe-containing formulae. The H/C ratio of <0.2, which was found for all Me-containing formulae in ESI positive mode, but not for any of the assigned unambiguous Cu- and Fe-containing formulae, is considered highly unlikely for naturally occurring organic compounds (Kind and Fiehn, 2007).

4. DISCUSSION

4.1. Cu dynamics in the STE

Sources and sinks of Cu in SB and WB: The Cu distribution patterns found in the two STEs indicate that groundwater can be a source for Cu to the coastal marine environment, as has been found elsewhere (Montluçon and Sañudo-Wilhelmy, 2001, Beck et al., 2010). However, deviations of Cu concentrations from Cu-salinity mixing curves occurred in both of the investigated STEs, namely a non-conservative decrease in the SB mid-beach station and a non-conservative increase in the WB LTWL station (Fig. 3). The WB dune station, which we consider as the most terrestrial (landward) groundwater source, was brackish and clearly not a pure fresh meteoric endmember. WB has a shorter beach width and faces the open North Sea, compared to SB dune which faces the more sheltered Wadden Sea. Thus chances of exposure to winter stormfloods were higher for this site, particularly when considering that WB was sampled in November and SB in August, and such floods likely diluted the terrestrial Cu endmember signal at this site.

Previously, non-conservative behavior of Cu concentrations in the STE had been attributed to more than one endmember from both, the terrestrial and the marine side (Charette and Buesseler, 2004, Beck et al., 2007). The slightly elevated Cu concentrations and a higher relative contribution of colloidal Cu in SB seepage compared to seawater (Fig. 3A) could point to such a deeper groundwater source. However, a relative increase in polycyclic aromates at SB LTWL indicative of a terrestrial source, as reported by Seidel et al. (2015), was not evident in our results (Fig. S1). In comparison, the Cu maxima at WB LTWL could be traced across the sediment-water interface into seepage and seawater (Fig. 3B), and furthermore co-occurred with elevated contributions of aromatic compounds pointing to a terrestrial origin, such as polycyclic aromates and polyphenol-type compounds (Fig. S1). Therefore, it is possible, that the high Cu levels at WB LTWL in part originated from a groundwater source which could not be sampled in "endmember quality" at the WB dune station. In addition, Spiekeroog contains buried peat layers at several locations (Streif, 2002). Such uncharted peat fragments in the intertidal zone could produce a terrestrial Cu (and DOM) signal in a brackish or even purely saline matrix.

It should also be noted that the seawater percolating though the USP and sampled in the mid-beach and LTWL

Table 3
Detected Fe- and Cu-DOM complexes in positive ionization mode, in comparison with reported complexes from known and newly identified ligands (citrate, salicylaldoxime, EDTA, 1, 2-nitroso-naphthol, ferrioxamine, ferrichrome, rhodotorulic acid). Ligand data from Gledhill (2001)$^{+}$, Waska et al. (2015)**, Waska et al. (2016)*, Boiteau et al. (2016)$^{++}$, and Chen et al. (2016)$^{\#}$. Compound groups are: unsat. + N = unsat. + N-like; sat. O/C-NSP = sat. O/Chydrate-like with N, S or P; sat. H/C-NSP = saturated fatty acid-like with N, S or P; BC-NSP = black sat. O/Cn-like with N, S or P; O-poor poly = Oxygen-poor polyphenol-like; O-poor h. unsat. = Oxygen-poor highly unsaturated compounds; O-rich h. unsat. = Oxygen-rich highly unsaturated compounds.

Fraction	m/z	Molecular formula	H/C	O/C	Compound group
NWA	237.0608	$C_9H_{18}NSCu(II)^+$	2.111	0.000	sat. H/C-NSP
	241.0557	$C_8H_{20}ONSCu(II)^+$	2.380	0.130	sat. H/C-NSP
	251.0765	$C_{10}H_{22}NSCu(II)^+$	2.100	0.000	sat. H/C-NSP
	255.0714	$C_9H_{22}ONSCu(II)^+$	2.333	0.111	sat. H/C-NSP
	263.0764	$C_{11}H_{22}NSCu(II)^+$	1.909	0.000	unsat. + N
	265.0557	$C_{10}H_{20}ONSCu(II)^+$	1.900	0.100	unsat. + N
	266.0873	$C_{10}H_{23}N_2SCu(II)^+$	2.200	0.000	sat. H/C-NSP
	267.0714	$C_{10}H_{22}ONSCu(II^+$	2.100	0.100	sat. H/C-NSP
	269.087	$C_{10}H_{24}ONSCu(II)^+$	2.300	0.100	sat. H/C-NSP
	277.0921	$C_{12}H_{24}NSCu(II)^+$	1.920	0.000	unsat. + N
	279.0713	$C_{11}H_{22}ONSCu(II)^+$	1.909	0.091	unsat. + N
	281.087	$C_{11}H_{24}ONSCu(II)^+$	2.091	0.091	sat. H/C-NSP
	281.0982	$C_{10}H_{24}N_3SCu(II)^+$	2.300	0.000	sat. H/C-NSP
	289.0921	$C_{13}H_{24}NSCu(II)^+$	1.769	0.000	unsat. + N
	293.0982	$C_{11}H_{24}N_3SCu(II)^+$	2.091	0.000	sat. H/C-NSP
	295.1027	$C_{12}H_{26}ONSCu(II)^+$	2.083	0.083	sat. H/C-NSP
	295.1139	$C_{11}H_{26}N_3SCu(II)^+$	2.273	0.000	sat. H/C-NSP
	301.0921	$C_{14}H_{24}NSCu(II)^+$	1.643	0.000	unsat. + N
	303.1078	$C_{14}H_{26}NSCu(II)^+$	1.786	0.000	unsat. + N
	305.087	$C_{13}H_{24}ONSCu(II)^+$	1.769	0.077	unsat. + N
	307.1027	$C_{13}H_{26}ONSCu(II)^+$	1.923	0.077	unsat. + N
	307.1139	$C_{12}H_{26}N_3SCu(II)^+$	2.083	0.000	sat. H/C-NSP
	309.0819	$C_{12}H_{24}O_2NSCu(II)^+$	1.917	0.167	unsat. + N
	309.1183	$C_{13}H_{28}O1NSCu(II)^+$	2.077	0.077	sat. H/C-NSP
	311.0976	$C_{12}H_{26}O_2NSCu(II)^+$	2.083	0.167	sat. H/C-NSP
	315.1078	$C_{15}H_{26}NSCu(II)^+$	1.667	0.000	unsat. + N
	317.087	$C_{14}H_{24}ONSCu(II)^+$	1.643	0.071	unsat. + N
	319.1027	$C_{14}H_{26}ONSCu(II)^+$	1.786	0.071	unsat. + N
	320.0979	$C_{13}H_{25}ONSCu(II)^+$	1.846	0.077	unsat. + N
	321.0819	$C_{13}H_{24}O_2NSCu(II)^+$	1.769	0.154	unsat. + N
	323.0976	$C_{13}H_{26}O_2NSCu(II)^+$	1.923	0.154	unsat. + N
	323.1088	$C_{12}H_{26}ON_3SCu(II)^+$	2.083	0.083	sat. H/C-NSP
	325.1132	$C_{13}H_{28}O_2NSCu(II)^+$	2.077	0.154	sat. H/C-NSP
	326.1449	$C_{13}H_{31}ON_2SCu(II)^+$	2.308	0.077	sat. H/C-NSP
	327.1078	$C_{16}H_{26}NSCu(II)^+$	1.563	0.000	unsat. + N
	329.087	$C_{15}H_{24}ONSCu(II)^+$	1.533	0.067	unsat. + N
	331.1027	$C_{15}H_{26}ONSCu(II)^+$	1.670	0.070	unsat. + N
	332.0979	$C_{14}H_{25}ON_2SCu(II)^+$	1.710	0.070	unsat. + N
	333.0819	$C_{14}H_{24}O_2NSCu(II)^+$	1.640	0.140	unsat. + N
	335.1088	$C_{13}H_{26}ON_3SCu(II)^+$	1.920	0.080	unsat. + N
	337.1132	$C_{14}H_{28}O_2NSCu(II)^+$	1.930	0.140	unsat. + N
	339.1077	$C_{17}H_{26}NSCu(II)^+$	1.470	0.000	O-poor h. unsat.
	343.1027	$C_{16}H_{26}ONSCu(II)^+$	1.560	0.060	unsat. + N
	349.1132	$C_{15}H_{28}O_2NSCu(II)^+$	1.800	0.130	unsat. + N
	349.1609	$C_{15}H_{32}N_3SCu(II)^+$	2.070	0.000	sat. H/C-NSP
	351.1289	$C_{15}H_{30}O_2NSCu(II)^+$	1.930	0.130	unsat. + N
	357.1183	$C_{17}H_{28}ONSCu(II)^+$	1.590	0.060	unsat. + N
	363.1765	$C_{16}H_{34}N_3SCu(II)^+$	2.060	0.000	sat. H/C-NSP
	376.1242	$C_{16}H_{29}O_2N_2SCu(II)^+$	1.750	0.130	unsat. + N
	379.1714	$C_{16}H_{34}ON_3SCu(II)^+$	2.060	0.060	sat. H/C-NSP
	500.1847	$C_{26}H_{32}N_5NaCu(I)^+$	1.192	0.000	O-poor h. unsat.
	674.3467	$C_{29}H_{61}O_8N_3SCu(I)^+$	2.069	0.276	sat. H/C-NSP
	675.2862	$C_{26}H_{55}O_{13}NNaCu(II)^+$	2.077	0.500	sat. H/C-NSP
	689.3018	$C_{27}H_{57}O_{13}NaCu(II)^+$	2.074	0.481	sat. H/C-NSP
	479.3582	$C_{22}H_3O_7NPMe^+$	0.091	0.318	BC-NSP
	483.3531	$C_{21}H_3O_8NPMe^+$	0.095	0.381	BC-NSP

Table 3 (*Continued*)

Fraction	m/z	Molecular formula	H/C	O/C	Compound group
	493.3738	$C_{23}H_5O_7NPMe^+$	0.174	0.304	BC-NSP
	497.3687	$C_{22}H_4O_8NPMe^+$	0.182	0.364	BC-NSP
	509.3687	$C_{23}H_5O_8NPMe^+$	0.174	0.348	BC-NSP
BSA	360.1006	$C_{17}H_{21}ON_4\ Cu(II)^+$	1.180	0.060	O-poor h. unsat.
	360.1370	$C_{18}H_{25}N_4\ Cu(II)^+$	1.330	0.000	O-poor h. unsat.
	374.1163	$C_{18}H_{23}ON_4\ Cu(II)^+$	1.220	0.060	O-poor h. unsat.
	374.1527	$C_{19}H_{27}N_4\ Cu(II)^+$	1.370	0.000	O-poor h. unsat.
	388.1319	$C_{19}H_{25}ON_4\ Cu(II)^+$	1.260	0.050	O-poor h. unsat.
	497.3137	$C_{10}H_4O_{17}NSMe^+$	0.400	1.700	O-poor poly
Ligands	336.0166	$C_{14}H_{13}O_4N_2Cu(II)^+$	0.929	0.286	O-poor poly*
	346.0094	$C_{10}H_{14}O_8N_2Fe(III)^+$	1.400	0.800	O-rich h. unsat.*
	398.0884	$C_{14}H_{22}N_4O_6Fe(III)^+$	1.571	0.429	unsat. + N^+
	391.9678	$C_{10}H_{14}O_8N_2KCu(II)^+$	1.400	0.800	O-rich h. unsat.*
	408.0166	$C_{20}H_{13}O_4N_2Cu(II)^+$	0.650	0.200	BC-NSP*
	470.9968	$C_8H_{17}N_2S_4Hg(II)^+$	2.125	0.000	sat. H/C-NSP$^{\#}$
	498.8868	$C_{12}H_{12}O_{14}Cu(II)Fe(III)^+$	1.000	1.167	sat. O/C*
	499.0282	$C_{10}H_{21}N_2S_4Hg(II)^+$	2.100	0.000	sat. H/C-NSP$^{\#}$
	572.0091	$C_{20}H_{21}O_8N_4S_2Cu(II)^+$	1.050	0.400	O-poor h. unsat.$^{++}$
	573.0619	$C_{30}H_{18}O_6N_3Fe(III)^-$	0.633	0.200	BC-NSP*
	614.2721	$C_{25}H_{46}O_8N_6Fe(III)^+$	1.800	0.320	unsat. + N**
	622.2746	$C_{25}H_{47}O_8N_6Cu(II)^+$	1.880	0.320	unsat. + N**
	698.2802	$C_{32}H_{54}O_6N_3S_2Ni(II)^+$	1.688	0.188	unsat. + N^{++}
	712.2959	$C_{33}H_{56}O_6N_3S_2Ni(II)^+$	1.697	0.182	unsat. + N^{++}
	741.2376	$C_{27}H_{43}O_{12}N_9Fe(III)^+$	1.593	0.444	unsat. + N^+

stations of both STEs is likely from a different season as it may take weeks to months for the infiltrated seawater to exfiltrate again (Seidel et al., 2015). Therefore, while fresh groundwater has longer travel times and is perhaps less variable over a seasonal scale, the Cu concentrations in the seawater endmember could fluctuate more rapidly due to natural (i.e. algal blooms, storms, precipitation, sediment re-suspension) and anthropogenic (i.e. from antifouling paints on ships, or discharge from rivers and groundwater drainage channels) impacts (Nolting, 1986, Charette and Buesseler, 2004), causing a time lag between the observed STE patterns and the adjacent coastal water column. Cu accumulating in marine sediments may also be a substantial source to the overlying water column. The elevated seepage Cu concentrations at SB compared to the water column concentrations, and the very high Cu concentrations in WB LTWL, thus might contain a substantial portion of exfiltrating USP water, driven by wave pumping or the landward hydraulic head (Nolting, 1986, Skrabal et al., 2000).

Finally, Cu in pore water of the STE may undergo cycles of co-precipitation and re-dissolution, as well as sorption-desorption to/from sulfides, clay particles, manganese oxides, or iron oxides. In line with these processes, we found a significant positive correlation of total Cu concentrations with those of total Fe concentrations across all WB STE stations ($p < 0.05$, $\rho = 0.61$), which indicate adsorption and release of Cu to and from Fe oxides (Kim and Kim, 2015). Such an association of Cu with iron oxides can be inhibited by complex formation of Cu with strong ligands, particularly at neutral to alkaline pH (Buerge-Weirich et al., 2002). Our voltammetric data indicate that Cu was organically complexed throughout both STEs and that Cu-binding ligands occurred in excess of the total dissolved Cu, thus potentially preventing Cu sorption. In addition, pH values throughout the STEs never fell below 7 (data not shown), in line with a recent study from Seibert et al. (2018) which found neutral to slightly alkaline pH values in the islands' freshwater lens.

It should be noted that in the STE, Cu(II) and Cu(I) likely coexist, particularly at the stations with high levels of reduced Fe(II) (in our case, SB-mid beach, SB LTWL, and WB LTWL). Reduction of Cu(II) to Cu(I) or perhaps even insoluble Cu(0) by Fe(II) was previously proposed to occur in an STE (Beck et al., 2010). Furthermore, under anoxic and sulfidic conditions, Cu(I)-polysulfides are likely the prevailing form of dissolved Cu (Skrabal et al., 2000). While we did not determine sulfide concentrations or Cu (I) species, we noted traces of sulfides as indicated by a weak sulfidic smell at both SB and WB LTWL stations, pointing to a likely occurrence of Cu(I)-sulfides. Of the stations with high abundances of reduced Fe(II), at WB LTWL the average Cu-ligand binding strengths, as calculated by CLE-ACSV, were slightly lower (average 11.93 $\pm$ 0.28), and the relative amounts of excess ligands (i.e. the % of free, unbound ligands compared to those bound to Cu), were substantially lower (% excess ligands = 23 $\pm$ 12), compared to the rest, including SB-mid beach and SB LTWL (average logK' = 12.30 $\pm$ 0.46, % excess ligands = 87 $\pm$ 8). In addition, the extraction efficiencies of organic Cu (NWA and BSA) were particularly low at this station, when regarding the high concentrations of total dissolved Cu (Fig. 3). Cu(I) complexes with small thiols like cysteine and glutathione have similar conditional stability

constants, but such small molecules have weak recoveries with SPE. Therefore it is likely, that substantial amounts of Cu at WB LTWL occurred as weakly bound organic and inorganic Cu(I) species, which could not be detected by CLE-ACSV, and not isolated using solid-phase extraction.

Speciation of Cu and the role of DOM: Our CLE-ACSV data show that organic complexation is a major parameter determining dissolved Cu distributions in the two Spiekeroog STEs, in line with a previous conclusion on Cu solubility in an STE (Beck et al., 2007). In SB STE, the significant positive correlation of DOC concentrations with those of total dissolved Cu ($p < 0.05$, $\rho = 0.59$) indicated that larger amounts of DOC (as proxy for DOM) could also sustain more Cu through stabilization in the mobile aqueous phase. However, in WB STE, no such correlation was found. DOC concentrations, as well as the CLE-ACSV-derived Cu-ligand pool, are bulk variables. As such, they do not always allow a direct inference on the quality of the organic matter which in turn could impact Cu complexing capacity. A combination of these bulk parameters with more detailed information on size classes, as well as chemical properties of extracted organic Cu enables a better understanding of the Cu-DOM dynamics in the STE. For example, the two respective stations in SB and WB STE with the highest amounts of DOC and Cu ligands, SB dune and WB LTWL, also had the highest total dissolved Cu concentrations, together with the highest relative share of colloidal Cu. SB dune and WB LTWL were also the only two locations where the Cu-BSA fractions were larger than the Cu-NWA fractions (Fig. 3). The BSA extraction (i.e. acidification of the sample) specifically targets aromatic, strong organic acids, which are typical for terrestrially-derived DOM groups such as humic substances. Throughout all analytical settings, the combined contributions of polycyclic aromates and polyphenols, i.e. the most aromatic DOM compound classes, were highest at SB dune and WB LTWL compared to all other stations (Fig. S1). Polyphenols are mainly produced by terrestrial, vascular plants as secondary metabolites and parts of structural entities such as lignins, also contributing to the humic substance pool (Kellerman et al., 2015). The negative correlations of polyphenol compound class abundances with salinity indicate a terrestrial (ground)water endmember as source of these compounds (Fig. S2). All these independently acquired data point to a common, terrestrial provenance of total dissolved Cu, colloidal Cu, and specific, vascular-plant derived terrestrial fractions of DOM. In line with our study, colloidal, humic-like DOM has been identified as a mobile Cu carrier in surface estuaries (Shank et al., 2004, Abualhaija et al., 2015). Cu bound to colloidal DOM may also be partly solid-phase extractable, because the colloids can be retained by "sticking" onto the SPE polymer surface, rather than partitioning in its pore spaces, and because some of the colloidal aggregates can be broken down during the SPE process (Waska et al., 2015, Broek et al., 2017). Thus, the organic colloidal Cu fraction may in part contribute to the extracted organic Cu fractions, as well as to the polyphenol compound classes detected in ESI-FT-ICR-MS.

In contrast to the SB dune and WB LTWL stations, at stations with a more marine character (i.e. higher salinities), such as WB mid-beach, and SB and WB seepage and seawater, total dissolved Cu concentrations were lower, colloidal Cu fractions were negligibly low, and extractable organic Cu consisted mainly of the NWA fraction. At these stations, compound classes with more aliphatic characteristics had their highest relative contributions to the molecularly described DOM pool (Fig. S1). It thus appears that Cu associated with typical marine DOM may play an increasingly important role on the way of SGD along the land-ocean gradient.

Overall, correlations between Cu distribution patterns and DOM parameters could indicate a variety of relationships, including a common provenance (e.g. groundwater *vs.* seawater), common geochemical regimes (e.g. oxic *vs.* anoxic), or direct interactions such as complex formation. For example, Cu ligand concentrations derived from CLE-ACSV on original water samples were significantly positively correlated with concentrations of the extracted Cu-BSA fraction ($p < 0.001$, $\rho = 0.69$), which could either mean that Cu is complexed by this component of DOM, or that they both have a common source. Furthermore, organic Cu extraction efficiencies changed with stations, geochemical regimes, and between SB and WB sites, indicating abundance shifts in the chemical fractions contributing to the Cu-binding ligand pool. However, the overall distributions of the two distinct extractable organic NWA- and BSA-Cu fractions confirm an overarching land-ocean trend from a terrestrial, organic acid, polyphenol-type ligand pool to one which is derived from marine organic matter (e.g. aliphatic, and N-containing).

Molecular properties of Cu-binding organic ligands: To the best of our knowledge, this study is the first to conduct in-depth analyses of FT-ICR-MS data in search for intact Cu-DOM complexes from an STE. The small number of Cu-DOM molecular formulae found amongst the tens of thousands of masses detected by the instrument for all of the analytical settings is likely due to the low concentrations of the Cu-DOM complexes (nanomolar concentrations of Cu, in comparison with micromolar concentrations of DOC) as well as the conservative knock-out criteria applied for molecular formulae assignments. While we still found several false positive formulae using our fake "Me" metal, they were much less abundant than those for Cu. This suggests that our conservative approach achieved a high probability of the Cu-containing formulae to be correct. Furthermore, using this method, we described the highest number of previously unknown complexes reported so far compared to other, environmental and experimental studies on trace metal-DOM complexation in natural waters (Boiteau et al., 2016, Chen et al., 2016, Waska et al., 2016).

All of the identified Cu-DOM formulae for all experimental settings were found to contain Cu(II), which would indicate that the stable, SPE-extractable organic Cu was also in a Cu(II) oxidation state. Most of the identified Cu-DOM formulae had elemental ratios of aliphatic, N-containing compounds typical for marine sources. The extraction and ionization mode favoring aliphatic,

N-(and S-)rich compounds, ESI positive ionization of the NWA fraction, is also the setting where most of the unambiguous Cu-DOM molecular formulae could be found (Table 3), and where the detection of "false positives" (5 Me complexes) was much less compared to that of unambiguous Cu-DOM compounds. Finally, elemental H/C and O/C ratios of the Cu-containing formulae were in the range of those of either long known, or recently described, complexes with trace metals such as Cu, Fe, Hg, or Ni (e.g. Boiteau et al., 2016, Chen et al., 2016, Waska et al., 2015, 2016). Their elemental ratios were also in the range of those molecular formulae which were significantly positively correlated with the amounts of extracted organic Cu (Fig. 5). This means, that correlating non-Cu containing molecules could (i) be potential Cu-binding but uncomplexed ligands, (ii) originate from the same (likely marine) source, or (iii) behave chemically similar to Cu-DOM complexes, either with regards to their distribution under specific STE geochemical regimes or with regards to their extractability and ionization efficiency under the tested analytical settings.

In addition, the relative abundances of several of the unambiguously assigned Cu-DOM molecular formulae were significantly negatively correlated with salinity, and the molecular formula with the strongest correlation was classified as a polyphenol-like compound indicative of terrestrial origin ($C_{25}H_{24}ON_4Cu(II)$, $p < 0.01$, $\rho = -0.56$, identified in the ESI negative ionization of the BSA fraction). These results confirm down to the molecular level, that terrestrially-derived humic-like DOM provides ligands for Cu and Fe in both surface and subsurface estuaries (Shank et al., 2004, Abualhaija et al., 2015). Our study is thus the first to provide evidence for the existence of such a complex directly within the unknown, natural DOM pool.

It should be noted that a large number of the described formulae in Tables 2 and 3 did not show abundance patterns indicative of specific water sources, STE types, or biogeochemical formation sites. To the best of our knowledge, only one other publication exists which reports a newly identified Cu-containing complex from natural DOM *via* FT-ICR-MS (Boiteau et al., 2016, Table 3). The complex was detected in samples from an open ocean environment with (significantly) different geochemistry and environmental conditions, but identified using an analytical approach similar to our ESI positive NWA setting, and it has an elemental composition similar to those of the compounds we found here. It is possible that SPE and FT-ICR-MS primarily target Cu-ligand complexes with different origins but similar chemical compositions and properties. As an example, siderophore-metal complexes are stable under low pH and can be solid-phase extracted in the BSA fraction, while weaker complexes, for example with humic substances, could be protonated and dissociated during SPE (Mills et al., 1982, Waska et al., 2015). One common denominator of preferentially solid-phase extractable compounds in the case of our study was the presence of N and S, perhaps in the form of Cu-binding functional groups. As FT-ICR-MS mainly provides elemental, but only limited structural information, it is not possible to infer how many structural isomers capable of binding Cu are hidden behind each assigned molecular formula. We therefore propose that in addition to site-specific indicator molecules such as the polyphenol-like complex from terrestrial groundwater in our study, a ubiquitous solid-phase extractable Cu-binding ligand pool may exist across aquatic boundaries, which is unified by similar trends in elemental characteristics (e.g., elevated H/C ratios, and presence of N and S).

4.2. Fe dynamics in the STE

Sources and sinks of Fe in SB and WB: Compared to Cu, which showed some indications of a land-ocean gradient, Fe abundances were even more difficult to delineate with regards to their sources, and most notably, characterized by non-conservative additions indicative of reductive Fe dissolution at the SB mid-beach and LTWL sites, and the WB LTWL site (Fig. 4). It is generally assumed that Fe in the STE originates from both, the terrestrial and the marine endmember (Charette and Sholkovitz, 2002), and that its solubility and mobility is closely related to its redox chemistry within the STE hydrological and geochemical zones. Environmental factors such as temperature, water saturation, organic matter quantity and quality, oxygen level, and residence time drive the microbial reductive dissolution of Fe(II). In addition, marine-derived phenolic compounds could reduce Fe(III) to Fe(II) even in oxic, sunlit waters prior to infiltration or shortly after exfiltration in and out of the beach (Santana-Casiano et al., 2010, 20014). Subsequently, tidal- and wave- driven oxic seawater infiltration, exfiltration of groundwater into oxic sediment layers, as well as microbial iron oxidation (McAllister et al., 2015), cause oxidative precipitation of Fe(III) ("iron curtain", Charette and Sholkovitz, 2002). At SB mid-beach, which is located approximately in the upper part of the USP (Fig. 1), infiltrating seawater should cause dissolved Fe depletion through oxidative precipitation in the upper sediment layers. Because our sampling commenced at 50 cm depth, and the campaign took place during summer, microbial respiration of oxygen and other electron acceptors such as nitrate, and subsequent reductive dissolution of Fe(II), must have occurred rapidly after infiltration, likely aided by marine organic debris: The SB mid-beach station was characterized by a marked macroalgal drift line, and carbohydrate analyses of the pore water underneath the drift line had revealed active microbial decomposition of labile marine organic matter in previous campaigns (Seidel et al., 2015). In addition, reduction of Fe(III) by phenolic compounds released from decomposing diatoms could be a so far unexplored mechanism beneath STE seawater infiltration sites (Santana-Casiano et al., 2014). On the other hand, high Fe(II) concentrations downstream, at SB and WB LTWL stations, are in line with the expectation of positive hydraulic gradients pointing upwards at these beach locations, enabling the upward advection of deep groundwater with long enough residence times to reduce and accumulate iron (Fig. 4, this study, Reckhardt et al., 2015).

Despite such high concentrations at the (presumed) discharge stations, adjacent seepage and seawater Fe concentrations were two- to four orders of magnitude lower than those in LTWL pore waters, and up to threefold lower than coastal North Sea Fe concentrations reported

previously (Nolting, 1986). In line with our findings, a drop in Fe concentrations similar to that at SB (approximately two orders of magnitude decrease between beach groundwater and surf zone seawater) was found for an STE in Patos Lagoon, Southern Brazil (Windom et al., 2006). Because sampling in our study commenced only from 50 cm sediment depth, we cannot trace the decrease of dissolved Fe in much spatial detail in the shallower sediment layers. Although our data indicate that the majority of the removal is due to formation of insoluble Fe oxides and Fe-humic coagulates, other processes may be important as well, for example the adsorption of Fe onto microbes attached to sediment grains or representing the particulate phase in the water column (Windom et al., 2006, González et al., 2014). Either way, strong gradients such as those in our study and in Windom et al. (2006) show the rapid decline of total dissolved Fe concentrations during passage through shallower sediment layers, and across the sediment-water interface.

Analogous to Cu, and in line with the higher LTWL pore water values, Fe concentrations in WB seepage and seawater were slightly higher compared to those at SB. However, not only was the difference between the two STEs larger for Cu, but also the decrease between the WB LTWL concentrations and those of the overlying seawater was less sharp for Cu compared to Fe (Figs. 3 and 4). These data indicate a more efficient transfer of Cu across the sediment-water interface compared to Fe. While both, Cu and Fe abundances, are impacted by some of the same processes, for example removal through iron oxide precipitation, or stabilization in solution through complexation with organic matter, it appears that in the case of Cu, the latter process may be more important than the former. We did not conduct voltammetric determinations of organic Fe complexation in the two STEs, but consider it unlikely that micromolar Fe concentrations can be sustained by the observed micromolar DOC concentration ranges (Table 1). Based on our data it appears that net fluxes of Fe across the sediment-water interface are rather small, and much of the Fe in these STEs simply undergoes recurring cycles of oxidation and reduction within the sediment body. This net flux may however be subject to seasonal changes of redox conditions in the benthic boundary layer, as well as influenced by changes in quality and quantity of supplied DOM.

Speciation of Fe and the role of DOM: Because CLE-ACSV was only conducted for Cu we cannot show directly to which degree Fe is organically complexed in the STE. However, our environmental parameters indicate that Fe in our study sites contained large inorganic contributions: At the stations with high levels of total Fe concentrations, those of Fe(II) and soluble Fe were elevated as well, yet the extraction efficiencies of organic Fe were lowest, and these low extraction efficiencies were found for all high-Fe stations of both, WB and SB (Fig. 4). Therefore, our results indicate that stations with high Fe concentrations are primarily release locations for reduced, soluble, and uncomplexed Fe(II), which is not recovered with the SPE method. In addition, overall extraction efficiencies for organic Fe (based on total dissolved Fe concentrations) were much lower compared to those for Cu, lower than those reported for siderophores from seawater or reagents of pure siderophore solutions (Macrellis et al., 2001, McCormack et al., 2003, Waska et al., 2015), and similar to those from another groundwater exfiltration site in the coastal North Sea (Waska et al., 2015). As abovementioned, these low extraction efficiencies can in part be explained by the high contributions of unbound, reduced Fe(II) to the total dissolved Fe pool. Another reason could be the substantial amounts of colloidal Fe (Fig. 4). SPE recovery of organic (Fe-)colloids is possible, but probably poor, and furthermore highly unlikely for inorganic Fe-oxide nano-colloids. When only taking soluble Fe concentrations as the base for the calculation of extraction efficiencies, they correspondingly increase several fold for both STEs. Nevertheless, because the overall extractable organic Fe concentrations were so low, we could not find any correlations between them and the DOM proxy DOC. Although DOM clearly impacts Fe dynamics by providing the electron donors necessary for the production of reduced Fe(II) (Reckhardt et al., 2015, Seidel et al., 2015), and by supplying ligands which enhanced organic Fe extractability (this study), DOC quantity was not a good predictor of total dissolved Fe distribution patterns.

Analogous to Cu, the extractable organic, likely terrestrially-derived, Fe-BSA fraction decreased in relative abundance with increasing marine influence in the two STEs (Fig. 4). However, while the Cu-NWA and Cu-BSA fractions showed completely contrasting patterns from each other in distribution (marine vs. terrestrial) and DOM molecular association (peptides vs. polyphenols) as revealed by the different analytical settings, the Fe-NWA fraction did not seem to be linked as clearly to a (marine) influence as Cu-NWA. The operational separation of "NWA" and "BSA" fractions is not clear-cut; it is probable that amphiphilic compounds can be recovered by both extraction techniques. The question is then, why NWA and BSA fractions correlating with extractable organic Cu concentrations show a larger differentiation in molecular composition compared to those correlating with extracted organic Fe.

Overall, extractable organic Cu-NWA was linked to a larger number of detected molecular formulae - two- to fivefold more than Fe-NWA (Figs. 5 and 6) – and these formulae were characterized by a higher degree of saturation in the former compared to the latter (Tables 2 and 3). Furthermore, Cu-NWA concentrations in SB STE were significantly positively correlated (ESI negative mode, $p < 0.001$, $\rho = 0.81$), while Fe-NWA concentrations were significantly negatively correlated (ESI negative mode, $p < 0.05$, $\rho = -0.56$), with relative abundances of N-containing aliphatics, a compound group associated with the marine endmember (Figs. 5 and 6). Both, Fe and Cu have been shown to form complexes with terrestrially-derived humic substances; such humic substances would correspond mainly to the BSA fraction, and the polyphenol compound class described here, likely containing high amounts of metal-binding carboxyl and hydroxyl functionalities (Koch et al., 2005, Batchelli et al., 2010, Abualhaija et al., 2015, Fig. S2, 6). In surface estuaries, Fe and Cu compete for humic substances, with Fe generally exhibiting

higher binding strengths compared to Cu, and Cu being more versatile in utilizing other, perhaps autochtonous organic ligand types supplied by algal and bacterial DOM (Muller and Batchelli, 2013, Abualhaija et al., 2015). In our STEs, Fe occurred in μM concentrations, compared to nanomolar concentrations of Cu. Together with a higher affinity for humic substances, as represented by the polyphenols here, high Fe abundances likely result in a closer association of Fe with more aromatic DOM even within the NWA fraction, while Cu is primarily linked with more aliphatic compound classes.

Molecular properties of Fe-binding organic ligands: Interestingly, all of the identified complexes in our study contained the reduced Fe(II). While reduction of Fe-complexes can occur at the ESI source during negative ionization, the molecular formulae could also be natural Fe(II)-ligand complexes formed by marine DOM and Fe released during reductive dissolution of Fe oxides in the STE. Although it is generally assumed that Fe(III) produces more abundant, more stable, and longer-lived complexes due of its additional binding site (Barbeau et al., 2001, Boiteau et al., 2013), Fe(II) complex formation has been proposed for high-Fe(II) environments such as hydrothermal vents (Kleint et al., 2017). Reductive dissolution of Fe(II) is a major process in STEs, and Fe(II) reduction may further proceed in the oxic, sunlit water column by phenolic exudates from diatoms (Santana-Casiano et al., 2014). Thus, our data shows first evidence that STEs may be significant formation sites of Fe(II)-DOM-complexes, in contrast to open ocean environments.

Another surprising result was that like Cu, extractable organic Fe concentrations had highly significant correlations with relative abundances of polyphenol compounds in DOM. But for Cu, at least one polyphenol ligand could be described with a molecular formulae, while none of the identified unambiguous, Fe-containing molecular formulae were polyphenols, but instead N-containing aliphatics and oxygen-poor, highly unsaturated compounds (Fig. 4, Tables 2 and 3) indicative of a marine provenance. This discrepancy is more striking for Fe, as it generally has a higher affinity for humic substances than Cu, and also occurred in much higher concentrations in our STEs (Table 1). Humic substances, to which terrestrially-derived polyphenols such as those found in our study contribute, form both, dissolved and insoluble (coagulated) complexes with Fe (Tipping, 1982, Batchelli et al., 2010, Linkhorst et al., 2017). The degree of Fe-humic coagulation is likely a function of Fe:DOC ratio (Kritzberg et al., 2014). We previously showed that iron oxide precipitation in the STE can trap terrestrially-derived polyphenols, and that the organic fraction of the Fe-DOM precipitates can be re-dissolved into FT-ICR-MS detectable, small polyphenols (Linkhorst et al., 2017). Thus, while Cu may be capable of forming small, soluble, FT-ICR-MS detectable (analytical window 200–2000 Da) complexes with polyphenol subunits, successive Fe-polyphenol aggregations could shift complex sizes into the colloidal fraction (>1kDa, Batchelli et al., 2010), which is less likely to be isolated by SPE or detected by ultra-high resolution mass spectrometry.

Overall, less Fe-containing molecular formulae were found compared to those with Cu. Due to the small natural abundance of the ^{54}Fe isotopologue (~6%), it is less likely to be detected compared to, for example, that of ^{37}Cl (24%) or ^{65}Cu (31%) or an average DOM compound with $^{12}C_{24}{}^{13}C_1$ (26%), especially in a complex DOM matrix. Therefore, the "dilution" of Fe concentrations amongst large numbers of DOM compounds affects it more that it does for Cu. The best chance of detecting Fe-containing compounds is if they are primarily bound to a restricted set of high-affinity ligands with high ionization efficiencies as shown for siderophores (Gledhill, 2001, Waska et al., 2015). Indeed, the unambiguous Fe-and Cu-containing formulae in our samples were aliphatic and contained nitrogen like known siderophores such as desferioxamine B ($C_{25}H_{48}O_8N_6$), ferrichrome ($C_{27}H_{42}O_{12}N_9Fe$) or rhodotoluric acid ($C_{14}H_{24}O_6N_4$) (Tables 2 and 3, Gledhill, 2001, Waska et al., 2016). It should be noted that so far, known siderophore-Fe complexes were predominantly detected in positive ionization mode due to their higher ionization efficiencies under this setting (Gledhill, 2001, Waska et al., 2015), while the Fe-containing formulae here were found exclusively in ESI negative mode. The absence of Fe-containing siderophore molecular formulae in ESI positive mode could be explained by our conservative elimination approach, which has a slight bias towards false negative results. As an example, the ferrioxamine-Fe complex, which had been added to some samples in trace amounts for internal calibration, was detected in ESI positive mode and assigned the correct formula, but also an additional, chemically sensible formula ($C_{27}H_{51}O_{10}NaFe(III)$), which excluded it from being detectable based on criterion 6 (non-unambiguous metal-containing formula assignment). As such, the unambiguous Fe-containing molecular formulae described in our study may simply be the small subsample of a large pool of novel, siderophore-type complexes found in subsurface and surface aquatic environments.

5. CONCLUSION AND OUTLOOK

In our study, we applied a novel method cross-over approach to investigate the role of DOM in Cu and Fe speciation in the subterranean estuary. Each of our complementary analytical windows added a layer of information on trace metal-DOM interactions, down to the molecular level, in this complex land-ocean interface. Based on our study, we propose that SGD can be a source for both Cu and Fe to the coastal ocean, but that the transfer across the sediment-water interface is more efficient for Cu than for Fe. We suggest that this is due to Fe being primarily associated with humic-like DOM in the form of immobile Fe-oxide-precipitates, while Cu may preferentially bind to autochtonous algal and microbial ligands which are more mobile across the STEs' redox zones. Furthermore, we propose that Fe-humic scavenging may be even higher in STEs compared to surface waters, because the high Fe:DOC ratio favors the formation of immobile complexes. In addition to co-variations of Cu and Fe with terrestrial and marine end-members, this would mean that analogous to surface estuaries, subterranean estuaries promote metal-ligand

exchange and selectively release small, aliphatic, N-containing Cu- and Fe-complexes into surface waters. This study was conducted at two sites with a substantial marine influence; it is well possible that in microtidal locations with a stronger terrestrial influence (hydraulic gradient as well as DOM composition and concentration), mobile Fe-humic and Cu-humic complexes may play a more important role. Nevertheless, our results imply that a sub-fraction of particularly stable metal-DOM complexes could exist across aquatic boundaries. We suggest that interdisciplinary analytics such as those applied here will substantially increase our current knowledge of metal-DOM interactions, and subsequently improve speciation models in ecohydrological interfaces and beyond.

ACKNOWLEDGEMENTS

We would like to thank Anja Reckhardt, Tania Röper, and Malte Groh for assistance with sampling on Spiekeroog. We are also indebted to Katrin Klaproth, Ina Ulber, and Matthias Friebe for support with analyses of DOC, TDN, and DOM molecular properties. Eleonore Gründken, Ann-Katrin Meinhardt, and Carola Lehners were of valuable help with nutrient analyses and trace metals analyses. Finally, we are indebted to two anonymous reviewers for their insightful and constructive comments. HW and HS were financially supported by a DFG "Eigene Stelle" fellowship to HW (WA 3067/2-1), as well as by the Ministry of Lower Saxony through project "BIME" (ZN3184).

APPENDIX A. SUPPLEMENTARY MATERIAL

Supplementary data to this article can be found online at https://doi.org/10.1016/j.gca.2019.06.004.

REFERENCES

Abualhaija M. M., Whitby H. and van den Berg C. M. (2015) Competition between copper and iron for humic ligands in estuarine waters. *Mar. Chem.* **172**, 46–56.

Barbeau K., Rue E. L., Trick C. G., Bruland K. W. and Butler A. (2001) Photochemical reactivity of siderophores produced by marine heterotrophic bacteria and cyanobacteria based on characteristic Fe(III) binding groups. *Limnol. Oceanogr.* **48**, 1069–1078.

Batchelli S., Muller F. L. L., Chang K. C. and Lee C. L. (2010) Evidence for strong but dynamic iron-humic colloidal associations in humic-rich coastal waters. *Environ. Sci. Technol.* **44**, 8485–8490.

Beck A. J., Tsukamoto Y., Tovar-Sanchez A., Huerta-Diaz M., Bokuniewicz H. J. and Sañudo-Wilhelmy S. A. (2007) Importance of geochemical transformations in determining submarine groundwater discharge-derived trace metal and nutrient fluxes. *Appl. Geochem.* **22**, 477–490.

Beck A. J., Cochran J. K. and Sañudo-Wilhelmy S. A. (2010) The distribution and speciation of dissolved trace metals in a shallow subterranean estuary. *Mar. Chem.* **121**, 145–156.

Beck M., Reckhardt A., Amelsberg J., Bartholomä A., Brumsack H. J., Cypionka H., Dittmar T., Engelen B., Greskowiak J., Hillebrand H., Holtappels M., Neuholz R., Köster J., Kuypers M. M. M., Massmann G., Meier D., Niggemann J., Paffrath R., Pahnke K., Rovo S., Striebel M., Vandieken V., Wehrmann A. and Zielinski O. (2017) The drivers of biogeochemistry in beach ecosystems: a cross-shore transect from the dunes to the low-water line. *Mar. Chem.* **190**, 35–50.

Boiteau R. M., Fitzsimmons J. N., Repeta D. J. and Boyle E. A. (2013) Detection of iron ligands in seawater and marine cyanobacteria cultures by high-performance liquid chromatography-inductively coupled plasma-mass spectrometry. *Anal. Chem.* **85**, 4357–4362.

Boiteau R. M., Till C. P., Ruacho A., Bundy R. M., Hawco N. J., McKenna A. M., Barbeau K. A., Bruland K. W., Saito M. A. and Repeta D. J. (2016) Structural characterization of natural nickel and copper binding ligands along the US GEOTRACES Eastern Pacific Zonal Transect. *Front. Mar. Sci.* **3**, 243. https://doi.org/10.3389/fmars.2016.00243.

Broek T. A. B., Walker B. D., Guilderson T. P. and McCarthy M. D. (2017) Coupled ultrafiltration and solid-phase extraction approach for the targeted study of semi-labile high molecular weight and refractory low molecular weight dissolved organic matter. *Mar. Chem.* **194**, 146–157.

Buck K. N. and Bruland K. W. (2005) Copper speciation in San Francisco Bay: a novel approach using multiple analytical windows. *Mar. Chem.* **96**, 185–198.

Buck K. N., Moffett J., Barbeau K. A., Bundy R. M., Kondo Y. and Wu J. (2012) The organic complextation of iron and copper: an intercomparison of competitive ligand exchange-adsorptive cathodic stripping voltammetry (CLE-ACSV) techniques. *Limnol. Oceanogr. Methods* **10**, 496–515.

Buerge-Weirich D., Hari R., Xue H., Behra P. and Sigg L. (2002) Adsorption of Cu, Cd, and Ni on goethite in the presence of natural groundwater ligands. *Environ. Sci. Technol.* **36**, 328–336.

Burnett W. C., Bokuniewicz H., Huettel M., Moore W. S. and Taniguchi M. (2003) Groundwater and pore water inputs to the coastal zone. *Biogeochemistry* **66**, 3–33.

Charette M. A. and Buesseler K. O. (2004) Submarine groundwater discharge of nutrients and copper to an urban subestuary of Chesapeake Bay (Elizabeth River). *Limnol. Oceanogr.* **49**, 376–385.

Charette M. A. and Sholkovitz E. R. (2002) Oxidative precipitation of groundwater-derived ferrous iron in the subterranean estuary of a coastal bay. *Geophys. Res. Lett.* **29**. https://doi.org/10.1029/2001GL014512.

Charette M. A. and Sholkovitz E. R. (2006) Trace element cycling in a subterranean estuary: Part 2. Geochemistry of the pore water. *Geochim. Cosmochim. Acta* **70**, 811–826.

Chen H., Johnston R. C., Mann B. F., Chu R. K., Tolic N., Parks J. M. and Gu B. (2016) Identification of mercury and dissolved organic matter complexes using ultrahigh resolution mass spectrometry. *Environ. Sci. Technol. Lett.*. https://doi.org/10.1021/acs.estlett.6b00460.

Cho H. M. and Kim G. (2016) Determining groundwater Ra end-member values for the estimation of the magnitude of submarine groundwater discharge using Ra tracers. *Geophys. Res. Lett.* **43**, 3865–3871.

Cho H. M., Kim G., Kwon E. Y., Moosdorf N., Garcia-Orellana J. and Santos I. R. (2018) Radium tracing nutrient inputs through submarine groundwater discharge in the global ocean. *Sci. Rep.* **8**. https://doi.org/10.1038/s41598-018-20806-2.

Dittmar T., Koch B. P., Hertkorn N. and Kattner G. (2008) A simple and efficient method for the solid-phase extraction of dissolved organic matter (SPE-DOM) from seawater. *Limnol. Oceanogr. Methods* **6**, 230–235.

Donat J. R., Statham P. J. and Bruland K. W. (1986) An evaluation of a C-18 solid phase extraction technique for isolating metal-organic complexes from central North Pacific Ocean waters. *Mar. Chem.* **18**, 85–99.

Gerringa L. J. A., Herman P. M. J. and Poortvliet T. C. W. (1995) Comparison of the linear Van den Berg/Ružić transformation and a non-linear fit of the Langmuir isotherm applied to Cu speciation data in the estuarine environment. *Mar. Chem.* **48**, 131–142.

Gledhill M. (2001) Electrospray ionization-mass spectrometry of hydroxamate siderophores. *Analyst* **126**, 1359–1362.

González A. G., Pokrovsky O. S., Jimenéz-Villacorta F., Shirokova L. S., Santana-Casiano J. M., González-Dávila M. and Emnova E. E. (2014) Iron adsorption onto soil and aquatic bacteria: XAS structural stdy. *Chem. Geol.* **372**, 32–45.

Johannesson K. H., Chevis D. A., Burdige D. J., Cable J. E., Martin J. B. and Roy M. (2011) Submarine groundwater discharge is an important net source of light and middle REEs to coastal waters of the Indian River Lagoon, Florida, USA. *Geochim. Cosmochim. Acta* **75**, 825–843.

Kellerman A. M., Kothawala D. N., Dittmar T. and Tranvik L. (2015) Persistence of dissolved organic matter in lakes related to its molecular characteristics. *Nat. Geosci.* **8**, 454–457.

Kim I. and Kim G. (2015) Role of colloids in the discharge of trace elements and rare earth elements from coastal groundwater to the ocean. *Mar. Chem.* **176**, 126–132.

Kim T. H., Waska H., Kwon E., Suryaputra I. G. N. A. and Kim G. (2012) Production, degradation, and flux of dissolved organic matter in the subterranean estuary of a large tidal flat. *Mar. Chem.* **142–144**, 1–10.

Kind T. and Fiehn O. (2007) Seven golden rules for heuristic filtering of molecular formulas obtained by accurate mass spectrometry. *BMC Bioinf.* **8**, 105.

Kleint C., Pichler T. and Koschinsky A. (2017) Geochemical characteristics, speciation, and size-fractionation of iron (Fe) in two marine shallow-water hydrothermal systems, Dominica, Lesser Antilles. *Chem. Geol.* **454**, 44–53.

Koch B. P., Witt M., Engbrodt R., Dittmar T. and Kattner G. (2005) Molecular formulae of marine and terrigenous dissolved organic matter detected by electrospray ionization Fourier transform ion cyclotron resonance mass spectrometry. *Geochim. Cosmochim. Acta* **69**(13), 3299–3308.

Koch B. P. and Dittmar T. (2006) From mass to structure: an aromaticity index for high-resolution mass data of natural organic matter. *Rapid Commun. Mass Spectrom.* **20**, 926–932.

Koch B. P. and Dittmar T. (2016) From mass to structure: an aromaticity index for high-resolution mass data of natural organic matter (Erratum). *Rapid Commun. Mass Spectrom.* **30**, 250.

Kritzberg E. S., Villanueva A. B., Jung M. and Reader H. E. (2014) Importance of boreal rivers in providing iron to marine waters. *PLOS One* **9**. https://doi.org/10.5061/dryad.hq8k8.

Kwon E. Y., Kim G., Primeau F., Moore W. S., Cho H. M., DeVries T., Sarmiento J. L., Charette M. A. and Cho Y. K. (2014) Global estimate of submarine groundwater discharge based on an observationally constrained radium isotope model. *Geophys. Res. Lett.* **41**, 8438–8444.

Lee D. R. (1977) A device for measuring seepage flux in lakes and estuaries Limnol. *Oceanogr.* **22**(1), 2140–2147.

Linkhorst A., Dittmar T. and Waska H. (2017) Molecular fractionation of dissolved organic matter in a shallow subterranean estuary: the role of the iron curtain. *Environ. Sci. Technol.* **51**, 1312–1320.

McAllister S. M., Barnett J. M., Heiss J. W., Findlay A. J., MacDonald D. J., Dow C. L., Luther, III, G. W., Michael H. A. and Chan C. S. (2015) Dynamic hydrologic and biogeochemical processes drive microbially enhanced iron and sulfur cycling within the intertidal mixing zone of a beach aquifer. *Limnol. Oceanogr.* **60**, 329–345.

Macrellis H. M., Trick C. G., Rue E. L., Smith G. and Bruland K. W. (2001) Collection and detection of natural iron-binding ligands. *Mar. Chem.* **76**, 175–187.

McCormack P., Worsfold P. J. and Gledhill M. (2003) Separation and detection of siderophores produced by marine bacterioplankton using high-performance liquid chromatography with electrospray ionization mass spectrometry. *Anal. Chem.* **75**, 2647–2652.

Mills G. L., Hanson, Jr., A. K. and Quinn J. G. (1982) Chemical studies of copper-organic complexes isolated from estuarine waters using C_{18} reverse-phase liquid chromatography. *Mar. Chem.* **11**, 355–377.

Montluçon D. and Sañudo-Wilhelmy S. A. (2001) Influence of net groundwater discharge on the chemical composition of a coastal environment: Flanders Bay, Long Island, New York. *Environ. Sci. Technol.* **35**, 480–486.

Moore W. S. (1999) The subterranean estuary: a reaction zone of ground water and sea water. *Mar. Chem.* **65**, 111–125.

Muller F. L. L. and Batchelli S. (2013) Copper binding by terrestrial versus marine organic ligands in the coastal plume of River Thurso, North Scotland. *Est. Coast. Shelf Sci.* **133**, 137–146.

Nolting R. F. (1986) Copper, zinc, cadmium, nickel, iron and manganese in the Southern Bight of the North Sea. *Mar. Poll. Bull.* **17**, 113–117.

Oksanen J., Blanchet F. G., Kindt R., Legendre P., Minchin P. R., O'Hara R. B., Simpson G. L., Solymos P., Stevens M. H. H. and Wagner H. (2013) *Vegan: community ecology package. R package version 2.0-7* http://CRAN.R-project.org/package=vegan.

Omanović D., Garnier C. and Pižeta I. (2015) ProMCC: an all-in-one tool for trace metal complexation studies. *Mar. Chem.* **173**, 25–39.

Reckhardt A., Beck M., Seidel M., Riedel T., Wehrmann A., Bartholomä A., Schnetger B., Dittmar T. and Brumsack H. J. (2015) Carbon, nutrient and trace metal cycling in sandy sediments: a comparison of high-energy beaches and backbarrier tidal flats. *Est. Coast Shelf Sci.* **159**, 1–14.

Riedel T. and Dittmar T. (2014) A method detection limit for the analysis of natural organic matter via Fourier transform ion cyclotron resonance mass spectrometry. *Anal. Chem.* **86**, 8376–8382.

Riedel T., Zak D., Biester H. and Dittmar T. (2013) Iron traps terrestrially derived dissolved organic matter at redox interfaces. *PNAS* **110**(25), 10101–10105.

Röper T., Kröger K. F., Meyer H., Sültenfuss J., Greskowiak J. and Massmann G. (2012) Groundwater ages, recharge conditions and hydrochemical evolution of a barrier island freshwater lens (Spiekeroog, Northern Germany). *J. Hydrol.* **454–455**, 173–186.

Röper T., Greskowiak J. and Massmann G. (2014) Detecting small groundwater discharge springs using handheld thermal infrared imagery. *Groundwater* **52**, 936–942.

Roy M., Martin J. B., Cable J. E. and Smith C. G. (2013) Variations of iron flux and organic carbon remineralization in a subterranean estuary caused by inter-annual variations in recharge. *Geochim. Cosmochim. Acta* **103**, 301–315.

Rue E. L. and Bruland K. W. (1995) Complexation of iron(II) by natural organic ligands in the Central North Pacific as determined by a new competitive ligand equilibration/adsorptive cathodic stripping voltammetric method. *Mar. Chem.* **50**, 117–138.

Sander S. G. and Koschinsky A. (2011) Metal flux from hydrothermal vents increased by organic complexation. *Nat. Geosci.* **4**, 145–150.

Santana-Casiano J. M., González-Dávila M., González A. G. and Millero F. J. (2010) Fe(III) reduction in the presence of catechol in seawater. *Aquat. Geochem.* **16**, 467–482.

Santana-Casiano J. M., González-Dávila M., González A. G., Rico M., López A. and Martel A. (2014) Characterization of phenolic exudates from Phaeodactylum tricornutum and their effects on the chemistry of Fe(II)-Fe(III). *Mar. Chem.* **158**, 10–16.

Seibert S. L., Holt T., Reckhardt A., Ahrens J., Beck M., Pollmann T., Giani L., Waska H., Böttcher M. E. m., Greskowiak J. and Massmann G. (2018) Hydrochemical evolution of a freshwater lens below a barrier island (Spiekeroog, Germany): the role of carbonate mineral reactions, cation exchange and redox processes. *Appl. Geochem.* **92**, 196–208.

Seidel M., Beck M., Riedel T., Waska H., Suryaputra I. G. N. A., Schnetger B., Niggemann J., Simon M. and Dittmar T. (2014) Biogeochemistry of dissolved organic matter in an anoxic intertidal creek bank. *Geochim. Cosmochim. Acta* **140**, 418–434.

Seidel M., Beck M., Greskowiak J., Riedel T., Waska H., Suryaputra I. G. N. A., Schnetger B., Niggemann J., Simon M. and Dittmar T. (2015) Benthic-pelagic coupling of nutrients and dissolved organic matter composition in an intertidal sandy beach. *Mar. Chem.* **176**, 150–163.

Sirois M., Coutourier M., Barber A., Gèlinas Y. and Chaillou G. (2018) Interactions between iron and organic carbon in a sandy beach subterranean estuary. *Mar. Chem.* **202**, 86–96.

Shank G. C., Skrabal S. A., Whitehead R. F. and Kieber R. J. (2004) Strog copper complexation in an organic-rich estuary: the importance of allochtonous dissolved organic matter. *Mar. Chem.* **88**, 21–39.

Skrabal S. A., Donat J. R. and Burdige D. J. (2000) Pore water distributions of dissolved copper and copper-complexing ligands in estuarine and coastal marine environments. *Geochim. Cosmochim. Acta* **64**, 1843–1857.

Snyder M., Taillefert M. and Ruppel C. (2004) Redox zonation at the saline-influenced boundaries of a permeable surficial aquifer: effects of physical forcing an the biogeochemical cycling of iron and manganese. *J. Hydrol.* **296**, 164–178.

Tipping E. (1982) The adsorption of aquatic humic substances by iron oxides. *Geochim. Cosmochim. Acta* **45**, 191–199.

Turner D. R., Achterberg E. P., Chen C.-T. A., Clegg S. L., Hatje V., Maldonado M. T., Sander S. G., van den Berg C. M. G. and Wells M. (2016) Toward a quality-controlled and accessible Pitzer Model for seawater and related systems. *Front. Mar. Sci.* **3**, 139. https://doi.org/10.3389/fmars.2016.00139.

van den Berg C. M. G. (1984) Conditional stability constants of complexes of copper(II) with natural organic ligands in seawater by cathodic stripping voltammetry of copper-catechol complex ions. *Mar. Chem.* **15**, 1–18.

Viollier E., Inglett P. W., Hunter K., Roychoudhury A. N. and van Cappellen P. (2000) The ferrozine method revisited: Fe(II)/Fe (III) determination in natural waters. *Appl. Geochem.* **15**, 785–790.

Waska H. and Kim G. (2011) Submarine groundwater discharge (SGD) as a main nutrient source for benthic and water-column primary production in a large intertidal environment of the Yellow Sea. *J. Sea Res.* **65**, 103–113.

Waska H., Koschinsky A., Ruiz-Chancho M. J. and Dittmar T. (2015) Investigating the potential of solid-phase extraction and Fourier-transform ion cyclotron resonance mass spectrometry (FT-ICR-MS) for the isolation and identification of dissolved metal-organic complexes from natural waters. *Mar. Chem.* **173**, 78–92.

Waska H., Koschinsky A. and Dittmar T. (2016) Fe- and Cu-complex formation with artificial ligands investigated by ultra-high resolution Fourier-transform ion cyclotron resonance mass spectrometry (FT-ICR-MS): Implications for metal-organic complex studies. *Front. Mar. Sci.* **3**, 119. https://doi.org/10.3389/fmars.2016.00119.

Windom H. L., Moore W. S., Niencheski L. F. H. and Jahnke R. A. (2006) Submarine groundwater discharge: a large, previously unrecognized source of dissolved iron to the South Atlantic Ocean. *Mar. Chem.* **102**, 252–266.

Zhang J. and Mandal A. K. (2012) Linkages between submarine groundwater systems and the environment. *Curr. Opin. Environ. Sustain.* **4**, 219–226.

Associate editor: Jerome Gaillardet